12-14-2015

Dielectric Characteristics of Microstructural Changes and Property Evolution in Engineered Materials

Jallisa Janet Clifford
University of South Carolina - Columbia

DIELECTRIC CHARACTERISTICS OF MICROSTRUCTURAL CHANGES AND PROPERTY EVOLUTION IN ENGINEERED MATERIALS

by

Jallisa Janet Clifford

Bachelor of Science
Benedict College, 2013

Submitted in Partial Fulfillment of the Requirements

For the Degree of Master of Science in

Aerospace Engineering

College of Engineering and Computing

University of South Carolina

2015

Accepted by:

Prasun Majumdar, Director of Thesis

Frank Chen, Reader

Tanvir Farouk, Reader

Lacy Ford, Senior Vice Provost and Dean of Graduate Studies

ACKNOWLEDGEMENTS

I would like to thank my advisor Dr. Prasun Majumdar, whom has guided me and provided me with his knowledge since I started my graduate studies at the University of South Carolina. I would like to express my gratitude to Dr. Kenneth Reifsnider who co-advised me until the spring of 2015. I would also like to thank Dr. Frank Chen and Dr. Tanvir Farouk for graciously agreeing to officially serve as the readers and providing their advice. I would like to acknowledge the financial support provided by the National Science Foundation (NSF Award #1210792) and NASA EPSCoR (Award # NNX13AD43A). I also thank my respected professors in the department of mechanical engineering for contributing to my academic preparation. As a part of the collaborative NSF project with Prof. Frank Chen's group, his graduate student Yu Chen manufactured and provided porous ceramic SOFC specimens for my work. A special thanks to the undergraduate students Mr. Hunter Goman and Mr. Kevin Epley who worked with me in the labs. My appreciation to fellow graduate students and staff in the SOFC center who have helped me along the way. Finally, I would like to express my gratitude towards my parents, my brother, and my extended family and friends who have continuously motivated and supported me.

ABSTRACT

Heterogeneous materials are increasingly used in a wide range of applications such as aerospace, civil infrastructure, fuel cells and many others. The ability to take properties from two or more materials to create a material with properties engineered to specific needs is always very attractive. Hence engineered materials are evolving into more complex formulations or heterogeneities in multiple disciplines. Design of microstructure at multiple scales controls the global functional properties of these materials and their structures. However, local microstructural changes do not directly cause a proportional change to the global properties (such as strength and stiffness). Instead, local changes follow a latent evolution process including significant interactions for the most of the life and only shows significant bulk property change prior to failure. Therefore, in order to understand property evolution of engineered materials and predict potential catastrophic failure, microstructural changes need to be effectively captured. Characterizing these changes and representing them by material variables will enable us to further improve our material level understanding.

In this work, we will demonstrate how microstructural features of heterogeneous materials can be described quantitatively using broadband dielectric spectroscopy (BbDS). The frequency dependent dielectric properties can capture the change in material microstructure and represent these changes in terms of material variables, such as complex permittivity. These changes in terms of material properties can then be linked to

a number of different conditions, such as increasing damage due to impact or fatigue. Two different broadband dielectric spectroscopy modes are presented: i) standard BbDS for measurements of bulk properties, and ii) continuous scanning mode (Scanning BbDS) to measure dielectric property change as a function of position across the specimen.

In this study, we will focus on both ceramic materials and fiber reinforced polymer matrix composites as test bed material systems. In the first part of the thesis, we will present how different micro-structural design of porous ceramic materials can be captured quantitatively using BbDS. These materials are typically used in solid oxide fuel cells (SOFC) as anode materials. Results show significant effect of microstructural design on material properties at multiple temperatures (up to 800 °C).

In the later part of the thesis, we will focus on microstructural changes of fiber reinforced composite materials due to impact and static loading. The changes in dielectric response can then be related to the bulk mechanical properties of the material and various damage modes. Observing trends in dielectric response enables us to further determine local mechanisms and distribution of properties throughout the damaged specimens. A 3D X-ray microscope and a digital microscope have been used to visualize these changes in material microstructure and validate experimental observations. The increase in damage observed in the material microstructure has been captured by the changes in BbDS characteristics. Results show that BbDS is an extremely useful tool for identifying microstructural changes within a heterogeneous material and particularly useful in relating remaining properties. For example, the remaining property (such as modulus) after low velocity impact shows significantly higher sensitivity to dielectric properties and hence provided a more accurate representation of material state change. This

sensitivity holds for both predominantly dielectric glass fiber to mixed conductor carbon fiber reinforced composite. The great advantage of using material variables is that these variable can be defined at multiple scales, and hence used directly in property degradation laws to help develop a framework for future predictive modeling methodologies.

TABLE OF CONTENTS

LIST OF FIGURES

CHAPTER 1
INTRODUCTION

Engineered materials are increasingly used in a wide range of applications such as aerospace, civil infrastructure, fuel cells and many others. The ability to take properties from two or more materials to create a material with properties tailored to your needs is always very attractive. Hence heterogeneous materials are evolving into more complex formulations in multiple disciplines. In the aerospace industry, we see that engineered materials are becoming increasingly popular in a wide variety of areas, this includes composite materials used for large aerospace structures, as well as, ceramic materials that have been used in engines and energy conversion devices. The microstructural design of these materials and their structures at multiple scales controls their global functional properties.

1.1 HETEROGENEOUS MATERIALS

A heterogeneous material is a non-uniform material composed of diverse parts that occupy the same volume. These dissimilar parts can then be distinguished from one another. The definition of heterogeneity is also often associated with a length scale (as the scale decreases, the same material can be treated as homogeneous or heterogeneous). A fundamental understanding and predictive capability is required in order to make material systems that have controlled shapes, properties, and interfaces that enable them to interact and act together as a system [1]. Heterogeneous functional materials are best

described as material systems that consist of multiple materials combined at scales from nano to macro that actively interact during their functional history in a manner that controls their collective performance as a system at the global level [2]. These materials interact with their environment to do one or more of the following things: conduct, emit, absorb, convert or alter them in various ways. These functional heterogeneous materials can be used in membranes and electrodes and in forms that make it possible to create critical medical, energy and material processing devices. These materials have quickly replaced homogeneous materials in many energy-centric devices that make electrochemistry, fuel synthesis, chemical refinement, hydrogen storage, and other essential processes possible. Design of heterogeneously functional materials begins with the requirements that drive the selection of the constituents [1].

1.1.1 Heterogeneous Ceramic Materials for Solid Oxide Fuel Cells (SOFCs)

Fuel cells are direct electrochemical energy conversion devices. They can be viewed as a device that transforms the chemical energy stored in a fuel directly into electrical energy. At a minimum, each fuel cell must contain two electrodes (an anode and a cathode) and one electrolyte [3]. One of the challenges is selecting the most efficient materials for each of these parts. Fuel cell electrodes must have electronic and ionic conduction capabilities, and they must facilitate electrochemistry by their catalytic properties [1]. Any candidate for fuel cell materials must not only deliver high performance but must also be stable and durable in the fuel cell environment [3]. Engineered materials are clearly a good choice for obtaining all necessary properties. We can then design our materials in such a way that all operational requirements are met for

each particular fuel cell component. The development and design of optimal heterogeneous functional materials for specific fuel cell applications is an area of ongoing research.

Solid oxide fuel cells (SOFCs) employ a solid ceramic electrolyte. Oxygen ions are the ionic charge carriers in an SOFC membrane. Solid oxide fuel cells run at temperatures that are typically higher than 600 degrees Celsius, however their advantage lies in their high efficiency and fuel flexibility. The most popular solid oxide fuel cell electrolyte material is Yittria-stabilized Zirconia (YSZ). In a SOFC, water is produced at the anode, therefore most commonly anode and cathode materials are different. Cathode materials for solid oxide fuel cells are typically mixed ion-conducting and electronically conducting ceramic materials. The most common engineered material for the SOFC anode is a Ni-YSZ cermet, where the nickel will provide electronic conductivity and catalytic activity and the YSZ provides ionic conductivity, thermal expansion compatibility, mechanical stability, and maintains the high porosity and surface area of the anode structure [3].

1.1.2 Fiber Reinforced Polymer Composite Materials

The main advantage of a composite material is the ability to obtain high strength and stiffness, combined with low density. For example, readily available carbon fiber composites can match the stiffness and strength of high-grade aluminum in all directions at less than two thirds of the density, and specialty grades have the ability to double the strength and stiffness of steel in the fiber direction. Other advantages include the ability

to tailor the composite layup for optimum strength and stiffness, improved fatigue life, corrosion resistance and even fewer detailed parts and fasteners [4]. They offer great fatigue and durability potential and can be very tolerant to a number of environmental effects.

Fiber reinforced polymer composite materials are made up of two major constituents, the fibers and the matrix; however other secondary constituents can be added for desired engineered functional properties. The fibers provide the strength and stiffness; they can be coated for increased bonding with the matrix and to protect against environmental degradation. The matrix acts as a binding material; it protects the fibers from abrasion, transfers loads between the fibers and provides interlaminar shear strength. Secondary materials can consist of fillers and additives that provide important properties for a particular application, such as resistance to fire, moisture or certain chemicals may be necessary. A lamina is a single layer arrangement of unidirectional or woven fibers impregnated in a matrix material. In general, a lamina is assumed to be orthotropic in its material coordinate system. The term laminate is used to describe a stack of lamina oriented in a specific manner to achieve the desired result. The laminate has a mechanical response that depends upon both the lamina properties and the stacking sequence.

Composite materials are designed to develop distributed damage consisting of various types of defects and even multiple breaks in the same reinforced fiber. Damage modes can be matrix cracks, fiber breaks, debonding, micro-buckling or delamination. Because composites are designed to develop this damage throughout their lives, initiation of isolated damage is not considered the end of life for a composite. In many cases, we

see that composites are designed to allow failure at different laminas, while the laminate is still carrying the load. Therefore, we can clearly determine that failure for composite materials is not a unique event, instead the evolution of damage is what will cause final global failure. As depicted in figure 1.1, composite damage evolution can be divided into different phases: initiation, accumulation and growth, and interaction. As damage accumulates within a composite, the microstructure will change. Understanding these changes in microstructure will help us to predict the mechanical response of the material after damage is induced.

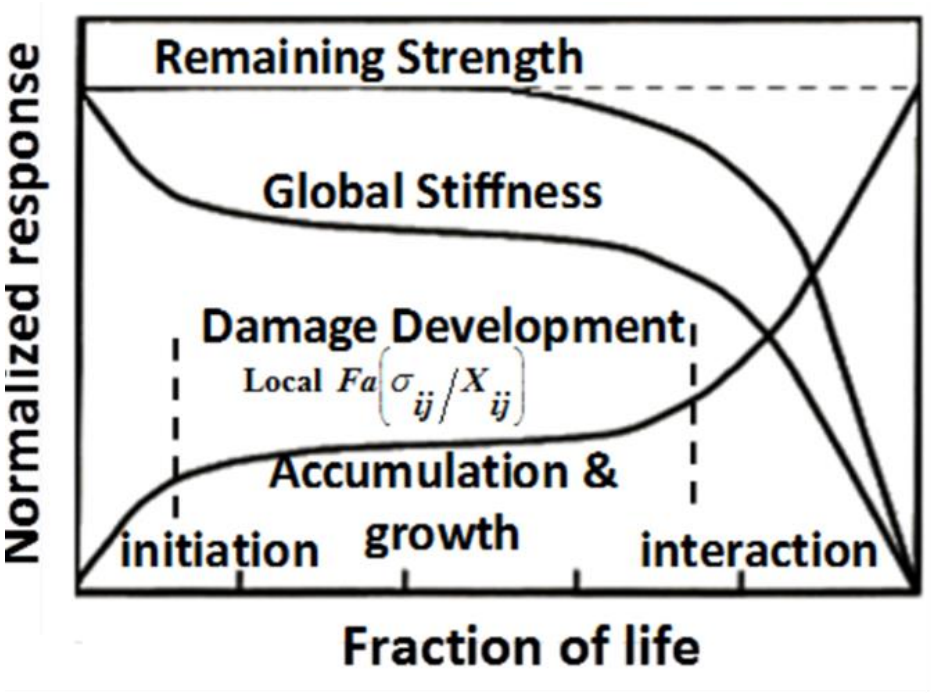

Figure 1.1 Stages of damage and remaining property evolution [5].

Barely visible impact damage (BVID) in composite materials has become a challenging problem in the aerospace industry. The increased use of composite materials in primary aerospace structures makes it important to understand the effects of low

velocity non-visible damage both immediately and long term. Low velocity impact can cause delamination (along with matrix cracks) beneath the surface, while the surface may appear to be undamaged upon visual inspection. The internal damage caused by impact may lead to an immediate reduction in properties (strength and stiffness) and the local delamination can slowly grow (for example, under cyclic loading) to affect durability. Therefore, an active area of research has come from the necessity to detect and monitor damaged below the BVID level [6]. Beyond the state of the art focus on detection of damage, the scientific challenge is to quantify the damage (material state change) and predict the corresponding changes in post-impact mechanical properties.

1.2 BROADBAND FREQUENCY DEPENDENT RESPONSE OF MATERIALS

1.2.1 Theoretical background

Dielectric properties of a material measure their ability to transmit electrical force, usually by storing energy in charge displacements that are "electrical springs". The charge displacements are called polarizations and the material property that defines that polarization, P, is called the susceptibility. The susceptibility can be associated with a number of different charge displacement mechanisms at various scales [7]. When heterogeneous dielectric materials are immersed in an electric field, electric charges accumulate at the discontinuity created by the interface between the different phases. This effect is known as Maxwell-Wagner-Sillars polarization and is an interfacial polarization at the mesoscopic scale [8].

The physics of this can be explained by the use of linear concept of currents, **J** and charge displacements, **D** in the presence of a vector electric field, **E** which may vary with time, and we state that

$$\mathbf{J} = \sigma \cdot \mathbf{E} \qquad \mathbf{D} = \varepsilon\varepsilon_o \cdot \mathbf{E} \tag{1}$$

Where σ is the conductivity of a given material phase, ε is the relative permittivity of that phase and ε_o is the permittivity of a vacuum. One can then invoke conservation of charge and the appropriate Maxwell's equation to obtain:

$$\nabla \mathrm{J} + \frac{d}{dt}(\Delta \mathrm{D}) = 0, \quad \mathrm{E} = -\Delta\phi' \tag{2}$$

Where ϕ' is the local point-wise potential value in the material. Then combining equations (1) and (2) we obtain the equation that controls the transient response as follows:

$$\nabla \cdot (\sigma \cdot \nabla\phi') + \frac{d}{dt}(\nabla \cdot (-\varepsilon\varepsilon_o \nabla\phi') = 0 \tag{3}$$

For steady state sinusoidal situations in which we can represent the potential as being the result of a harmonic input

$$\phi \cdot e^{iwt} \tag{4}$$

We find another form of equation (3)

$$\nabla \cdot \left[\left((\sigma + i\omega\varepsilon\varepsilon_o) \cdot \nabla\phi\right)\right] = 0 \tag{5}$$

Where ω is the frequency of the input signal.

Equation (5) demonstrates that in a heterogeneous material the product of the physical properties and the slope of the potential must be constant as we cross material

boundaries. The interacting field is a result of the charge in the electric field at the interface, and unless the conductivity and permittivity of adjacent material phases are identical, there is a disruption of charge transfer at the material boundary which results in internal polarization.

In the presence of an electric field, the potential in a homogeneous material has constant slope. If the second phase is added to create a composite element, and if the second phase has either higher conductivity or larger dielectric charge displacements, then the slope of the potential is altered. The contact product term in equation (5) indicates that the field changes within the material. From Gauss's law we know that the change in slope of the potential across a boundary is proportional to the surface charge, therefore when a more conductive material is inserted in our control volume we can conclude that the global capacitance will increase in proportion to the change in slope [8].

Extensive experimental validations performed by J. Baker at el. confirm that large variations in dielectric response can be designed and achieved for heterogeneous materials. In Baker's work, a foundation for rational design of dielectric response of heterogeneous materials is presented [8].

1.2.2 Experimental technique to measure frequency dependent response

Dielectric spectroscopy measures the dielectric properties of a medium as a function of frequency. It is based on the universal property of a substance to respond to an external electrodynamic action. The value and the temporal delay of a response as functions of the action are expressed in terms of measurable quantities, which are

determined only by the microscopic properties of a substance in the linear approximation. A dielectric response is expressed particularly in terms of real and imaginary parts of dielectric permittivity, the refractive index, the dielectric modulus, the absorption coefficient, or the conductivity. The dielectric permittivity is the most fundamental quantity; it enters the constitutive relations and is directly related to theoretical models [9].

Modern equipment allows measurements of dielectric response ranging from ultra-low frequencies to optical frequencies. Many different methods can be used for this wide frequency band. These methods can be divided in to two different categories, namely, impedance (contact) methods and high frequency optical methods. In low-frequency methods, metal electrodes are placed on either side of the specimen surface to launch the field into the specimen.

Broadband dielectric spectroscopy (BbDS) studies the interaction of electromagnetic waves with matter in the frequency range from 10^{-6} to 10^{12} Hz. This range is able to provide information about the molecular and collective dipolar fluctuations and about charge transport and polarization effects that occur at inner and outer boundaries. However, an extensive research by Prof. Reifsnider and Dr. Majumdar group [35-38] has shown that microstructural changes can be captured in the low frequency range (from 0.01 to 1 MHz) for a wide range of engineered materials such as ceramics and fiber reinforced composite. In this study a dielectric spectroscopy unit by Novocontrol Inc. will be used. In this equipment, the sample is mounted between two electrodes forming a sample capacitor. A voltage (U_0) with a fixed frequency ($\omega/2\pi$) is applied to the sample capacitor and the voltage causes a current (I_0) of the sample

frequency in the sample. There is also a phase shift present between the voltage and the current that is described as the phase angle (φ). The ratio between the voltage, current and the phase angle is determined by the sample material electric properties (permittivity and conductivity) and by sample geometry. The relations between these parameters are expressed as follows:

$$U(t) = U_0 \cos(\omega t) = Re(U * \exp(i\omega t)) \quad (1)$$

$$I(t) = I_0 \cos(\omega t) = Re(I * \exp(i\omega t)) \quad (2)$$

With $U^* = U_0$ and $I^* = I' + iI''$, where $I_0 = \sqrt{I'^2 + I''^2}$ and $\tan(\varphi) = \frac{I'}{I''}$. The measured complex permittivity can be calculated by:

$$\varepsilon^*(\omega) = \varepsilon' - i\varepsilon'' = \frac{-i}{\omega Z'(\omega)} * \frac{1}{C_0} \quad (3)$$

Here C_0 is the capacity of the empty sample capacitor.

The specific conductivity is:

$$\sigma^*(\omega) = \sigma' - \sigma'' = i2\pi f \varepsilon_0(\varepsilon^* - 1) \quad (4)$$

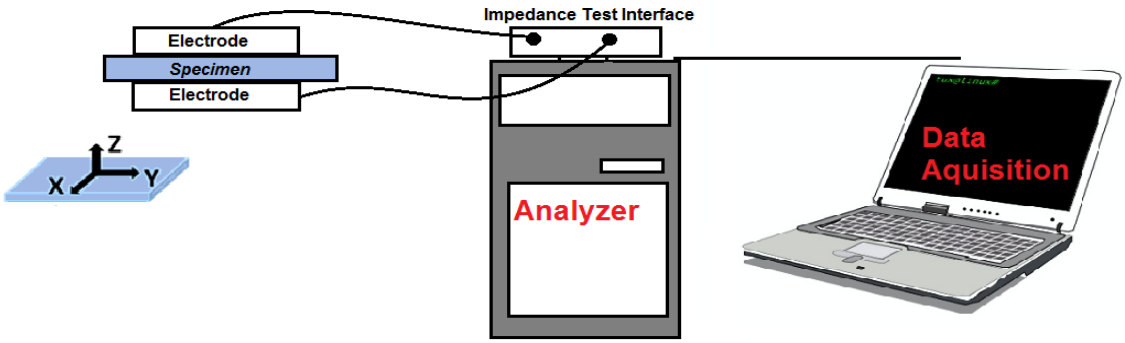

Figure 1.2. Schematic diagram of BbDS test setup.

1.3 VISUALIZATION OF MICROSTRUCTURE AND IMAGE BASED ANALYSIS

Visualization tools are needed to examine microstructural changes within a heterogeneous material. There are many traditional imaging techniques that provide 2D images of material microstructure. Amount the most common 2D imaging techniques are visualization through optical microscope, scanning electron microscopy (SEM) and transmission electron microscopy (TEM). SEM analyses the surface of materials so that fine details can be measured and assessed via image analysis. A scanning electron microscope scans a sample with a focused beam of electrons. The electrons interact with atoms in the samples, producing various signals that can be detected and translated to information regarding the surface tomography and composition. The electron beam is scanned in a raster scan pattern, and the beam's position is combined with the detected signals to produce an image. TEM is a microscopy technique that uses a beam of electrons that are transmitted through a specimen, interacting with the specimen as it passes thought. For this technique to work the specimen must be very thin. An image is then formed from the interaction of the electrons transmitted through the specimen. The image is then magnified and focus onto an imaging device.

Ultrasonic testing, acoustic emission and X-rays have proven to be effective non-destructive visualization methods. Ultrasonic testing uses information from the propagation of ultrasonic waves in the material being tested. In general very short waves are transmitted into the material to detect internal flaws or to characterize the material. This kind of testing is often performed on metals and alloys, but has also had some success being used on composite materials with less resolution. On the other hand, acoustic emission tools are designed to monitor acoustics emissions produced within the

material during failure or stress, instead of actively transmitting waves, then collecting them after they have traveled through the material. For material under active stress, for example some components of an airplane during flight, transducers mounted in an area can detect the formation of a crack at the moment it begins propagating. A large group of transducers are able to record signals, and then locate the precise area of their origin by measuring the time for the sound to reach different transducers.

3D X-ray spectroscopy is an advanced non-destructive visualization method. It uses computed tomography (CT) to create 3D datasets. Micro-computed tomography (micro-CT) delivers images with micrometer size pixels. This technique is advantageous because it enables us to obtain high resolution, three dimensional images of the damage or voids within a composite material. It enables us to capture micron size defects within an engineered material without the need for any physical de-layering or cross-sectioning. Advanced X-ray microscopy equipment has the ability to maintaining high resolution even at large working distances, and hence enabling imaging of larger specimens. 3D X-ray microscopy is ideal for nondestructive visualization and characterization of microstructure.

Table 1.1 Resolution and field of view at different magnifications in 3D X-ray Microscope

Magnification Level	Spatial Resolution Range (μm)	3D Field of View (mm)
1X	9 – 22	4 - 15
4X	5 – 6	2.4 – 6
10X	1.5	2 – 2.7

1.4 ORGANIZATION OF THESIS

In this work we will use broadband dielectric spectroscopy to quantitatively capture the change in different porous micro-structural designs of engineered ceramic materials commonly used in solid oxide fuel cells. 3D X-ray microscopy is then used to characterize the porous microstructure and link it to material variables obtained from dielectric spectroscopy. A literature review, experimental procedures, results and discussions for these findings can be seen in chapter two of this thesis. In the later portion of this work we will highlight the microstructural changes of fiber reinforced composites due to impact. The changes in dielectric response of the impacted specimens are then linked to the residual mechanical properties of the composite material. Damage areas of impacted specimens are visualized and compared to dielectric and mechanical results. A literature review, experimental procedures, results and discussions for this work can be seen in chapter three of this thesis. In chapter four of this thesis one can find procedures and results from various test cases that will help us understand how dielectric properties can be interpreted to determine the location and mode of damage within composite structures. Finally chapter five will highlight conclusions and will give insight on ongoing and future work.

CHAPTER 2

CHARACTERIZATION OF POROUS CERAMIC MICROSTRUCTURE AND ITS EFFECTS ON DIELECTRIC PROPERTIES

2.1 BACKGROUND

A literature review has been conducted to determine how ceramic microstructure has previously been characterized and liked to manufactured properties of the material. Many methods depend upon a fabrication process that gives a constant microstructural composition that may be found to be superior to the next. However, within each of those particular microstructural compositions there may be slight variations that have some effect on the material behavior. Chen [10] demonstrates that using a freeze-drying tape-casting and drop-coating manufacturing method a porous ceramic electrolyte with a graded open and straight microstructure is obtained. With the use of SEM Chen was able to determine pore size on the bottom and top surface, along with porosity distribution in the thickness direction and tortuosity factor. The novel microstructure created was expected to facilitate gas diffusion in the anode during operation and results showed good performance at low temperature ranges.

Previous works have shown that there are multiple physics involved in SOFC materials design, manufacturing, operation, degradation and performance [11]. To date a large amount of effort has been placed on electro-chemistry and materials research concerning searching for novel material behavior starting at a molecular level. However there is limited research concerning how morphological features contribute to as

manufactured properties [11]. In a study performed by Lanzini et al [12], microstructural characterization of SOFC electrodes was performed based on 2-D images. This work aimed to find a reliable description of the electrode structure using microscopic analysis performed by means of both SEM and an optical microscope. Lanzini had to use detailed mathematical methods to reconstruct the 3D structure of both fuel and air electrodes having 2D images as input.

Literature is lacking in the area of quantitatively describing ceramic porous microstructure in a simplistic and accurate manner that can be directly related to practical material variables. The objective of this experiment is to successfully characterize fuel cell anode material microstructure and porosity and relate it to dielectric properties using broadband dielectric spectroscopy. It is important to note that dielectrics show various properties at different, voltages, temperatures, frequencies, moisture content and mechanical stress [13]. Therefore, in this study we will consider frequency dependent results at a set temperature for our materials. This will help us determine how changes in microstructure for solid oxide fuel cell anode material will affects fuel cell performance and will aid in determining what porous structure is best suited for solid oxide fuel cell applications. Information regarding the microstructure of the solid oxide fuel cell material will aid in enabling higher fuel cell efficiency and lower solid oxide fuel cell operating temperatures.

2.2 EXPIREMENTAL PROCEDURE

2.2.1 Sample Size, Type and Preparation

In this experiment two different materials are examined: 25 percent volume fraction Ni-GDC and 25 percent volume fraction Ni-YSZ. In both cases the samples are

prepared in house by a freeze-drying tape casting process. In this process an aqueous ceramic slurry is first prepared and then casted onto a Mylar carrier film. After solidification, the tape is punched and freeze dried under a vacuum for a quick solvent removal through sublimation. This method creates a porous structure ideal for gas delivery in SOFC electrodes.

For use in the BbDS Unit the specimens must be disk shaped with a 12mm to 15mm diameter. Thickness of the specimens ranges from 0.2mm to 0.4mm. After the ceramic samples are prepared they must be coated with a conductive layer before being placed between the two mesh electrodes for dielectric testing. Both silver and platinum pastes have been used for this conductive layer depending on the temperature requirements.

2.2.2 High Temperature Broadband Dielectric Spectroscopy Testing

Dielectric measurements of our specimens at various temperatures ranging from room temperature to 1000 degrees Celsius have been taken. The dielectric properties of these materials are seen to be frequency depending and therefore a frequency range of 0.1Hz to 1MHz has been examined in every case. Broadband dielectric spectroscopy is used to determined dielectric characteristics of the ceramic materials. The BbDS unit used is by Novocontrol America Inc. For this experiment a temperature controller module is used to apply a variable amount of power to the furnace. This power is applied until the furnace or sample reaches the desired set-point. The unit includes the signal channels for the channel and furnace temperature sensors, a digital temperature controller with furnace

supply unit, the user display, 6 control keys and two line power switches. The software used with this device is WinDETA. WinDETA measures minor changes in material properties as it is subject to a periodic electrical field in order to characterize its molecular kinetics. In order to measure as much as quantitative data the BbDS hardware and software cover a broad range of frequency and temperature range.

As depicted in figure 2.1, the sample (disk shaped) is mounted into a ceramic tube along with the electrodes on either side of the sample and a thermocouple to accurately determine the samples temperature at all times.

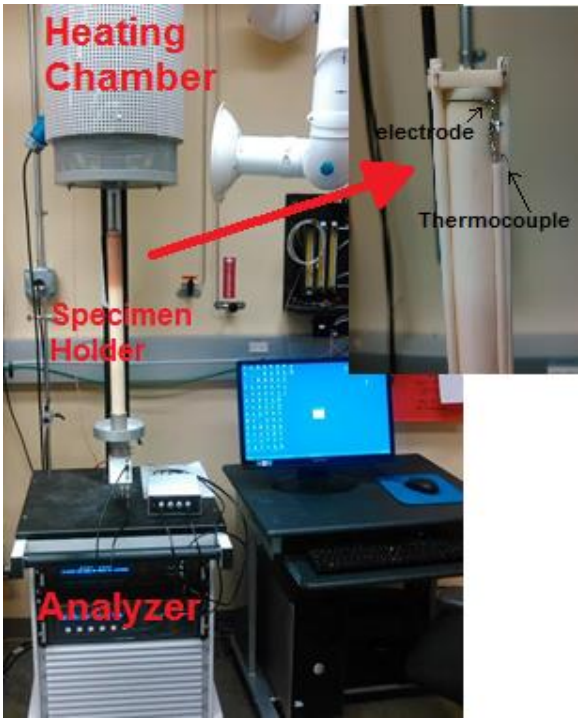

Figure 2.1.Novocontrol spectroscope with high temperature specimen holder.

2.2.2 Visualization and Microstructure Characterization

After dielectric testing is performed the samples are subject to non-destructive microstructure visualization using a 3D X-ray microscope. The 3D X-ray microscope

used is a Zeiss MicroXTC-400. The MicroXTC-400 has imaging at sub-1 micron pixel resolution and is equipped with a number of lenses allowing for different magnifications and varying fields of view. The major advantage of this equipment is that it allows for high spatial resolution with less sacrifice of field of view and a larger working distance.

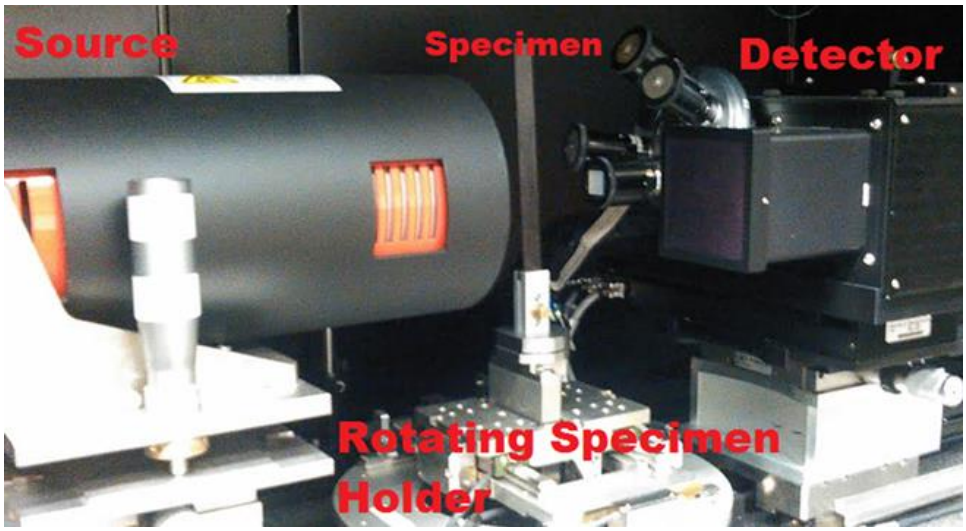

Figure 2.2. 3D X-ray microscope test setup.

After images have been taken via 3D X-ray microscope they are further examined using image processing software. This software allows us to segment the image so that we can accurately determine porosity and identify pore shapes and sizes. It is in this manner that we are able to characterize our porous microstructure and compared to dielectric properties taken for our specimen.

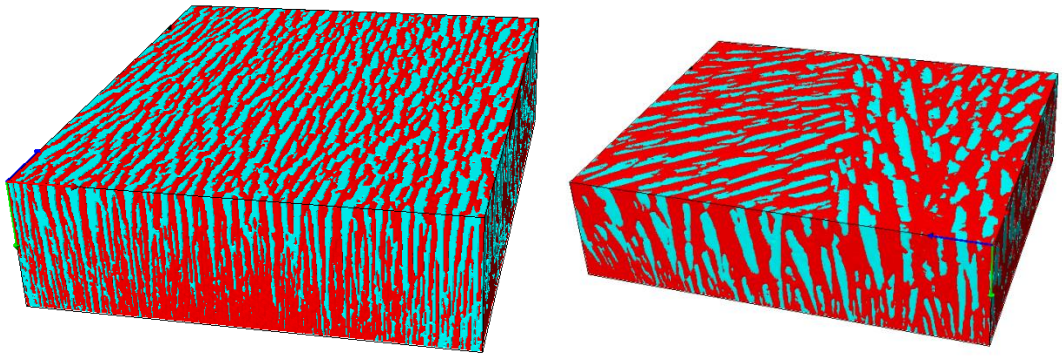

Figure 2.3. 3D image segmentation of porous ceramic microstructure.

2.3 RESULTS AND DISCUSSIONS

In this experiment the pore morphology is characterized by the porosity as well as the pore shape, thickness and orientation. Pores can be effectively characterized in terms of pore length, pore orientation, pore width and shape. Pore shape can fall into two categories either cone or cylindrical. Cone or cylindrical shapes are determined based on the change in pore size throughout the structure. If the pore size remains approximately the same on average the pores are concluded to be cylindrical, however if the pores are much larger at the surface and get narrower throughout the structure pores can be said to be cone shaped.

The first sample Ni-YSZ1, has a porosity of 24.6% and pores that go through the entire width of the sample. The average pore width is 0.032mm and the average pore width at the surface of the button cell is 0.037. The pores of this sample are of random orientation with both cone and cylindrical shape. A second sample Ni-YSZ2 has a higher porosity at 31.0% and pores that are also present through the entire width of the sample. In this case the average pore width is larger at 0.046mm and the pore width at the surface

is much larger at 0.065mm. The pores are cone shaped and oriented between 95 to 120 degrees. The microstructure of these two specimens can be seen in figure 2.4 below.

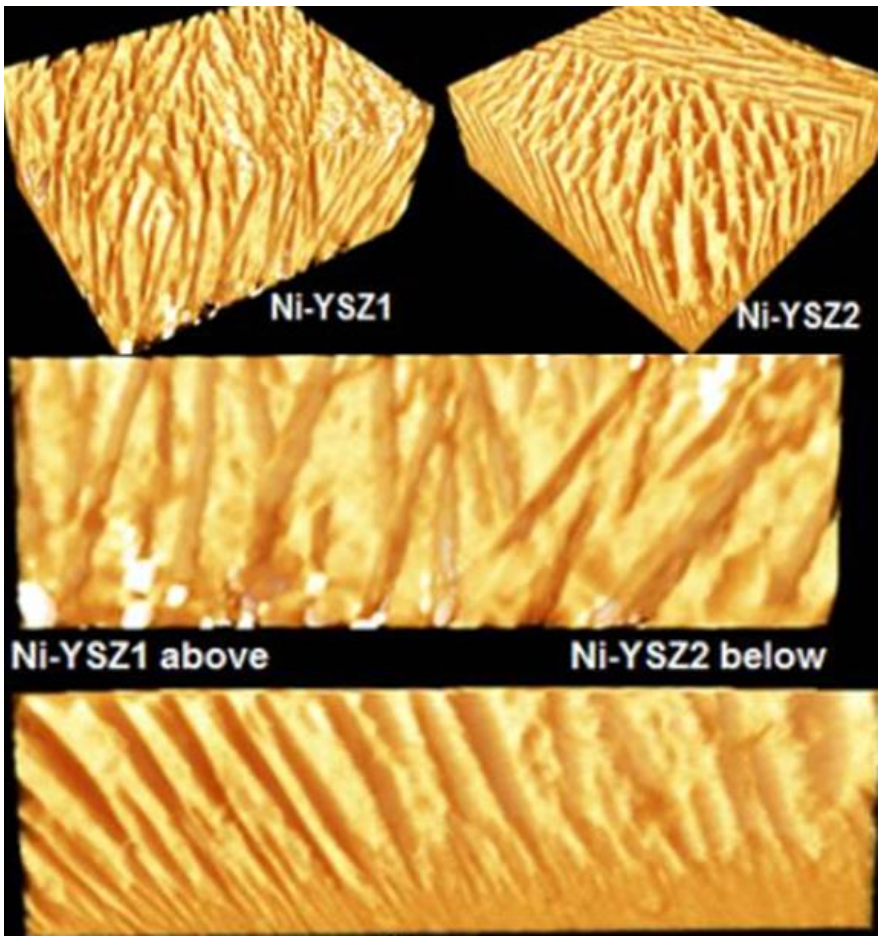

Figure 2.4. 3D X-Ray Image of Ni-YSZ1 and Ni-YSZ2 Microstructure.

After proper microstructure characterization we can now relate these porous geometries to dielectric properties of the ceramic material. As seen in the plotted results in figure 2.5, the higher porosity and larger pore size at the surface of the SOFC electrode material allows for higher conductivity.

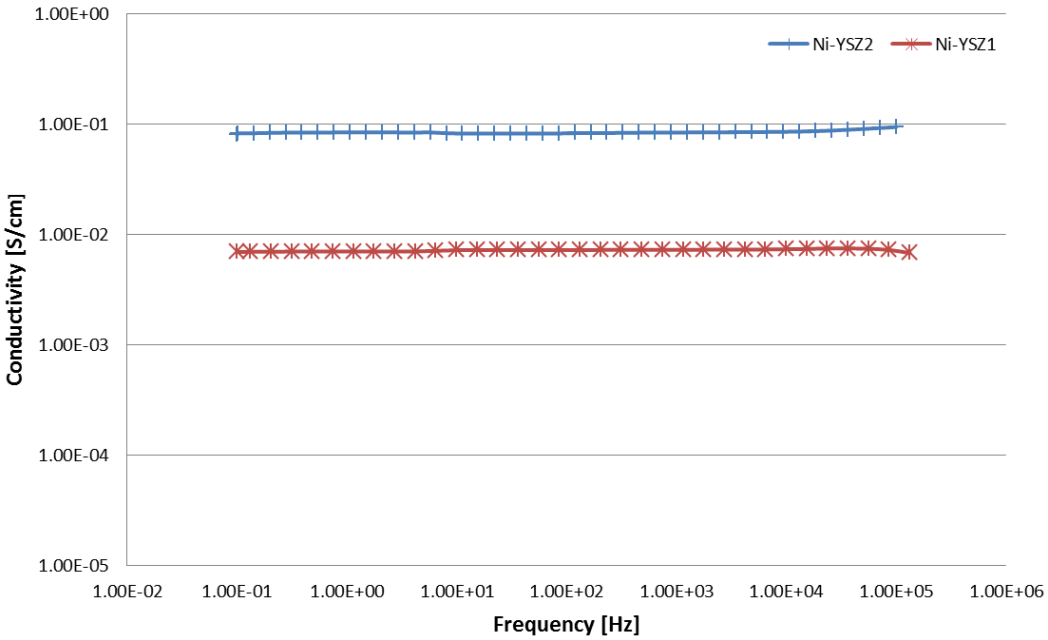

Figure 2.5. Ni-YSZ1 and Ni-YSZ2 conductivity as a function of frequency.

We can characterize Ni-GDC1 and Ni-GDC in the same manner we did Ni-YSZ1 and Ni-YSZ2 using Scan IP image processing software.

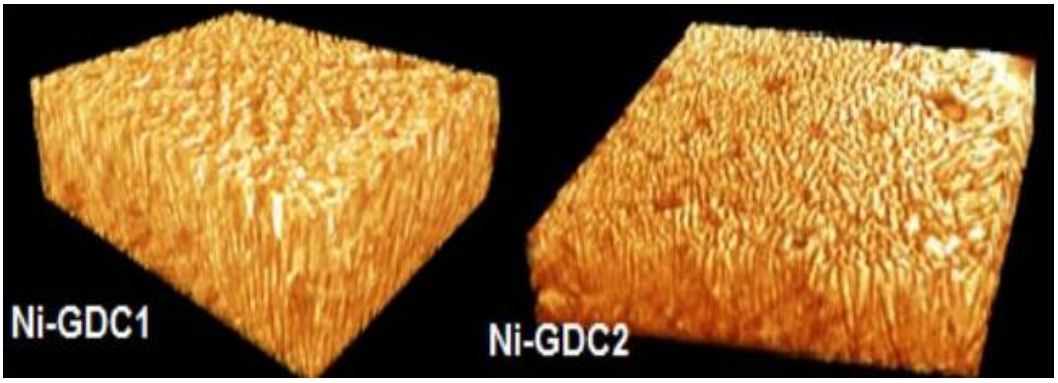

Figure 2.6. 3D X-ray images of Ni-GDC porous Microstructure.

For these samples the porosities are 30.0 and 31.6 respectively, however the average pore width for Ni-GDC1 is 0.039mm and the average pore width for Ni-GDC2 is much smaller at 0.015mm; the average pore widths at the surface are also 0.053mm and 0.022mm respectively.

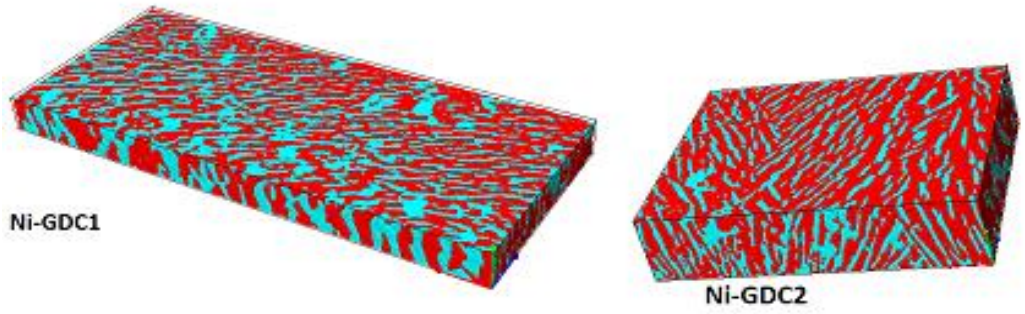

Figure 2.7. Segmented images of Ni-GDC microstructure.

We can now compare dielectric properties to the properly characterized microstructure of the Ni-GDC specimens. In this case we will examine impedance results 700 degrees Celsius as a function of frequency.

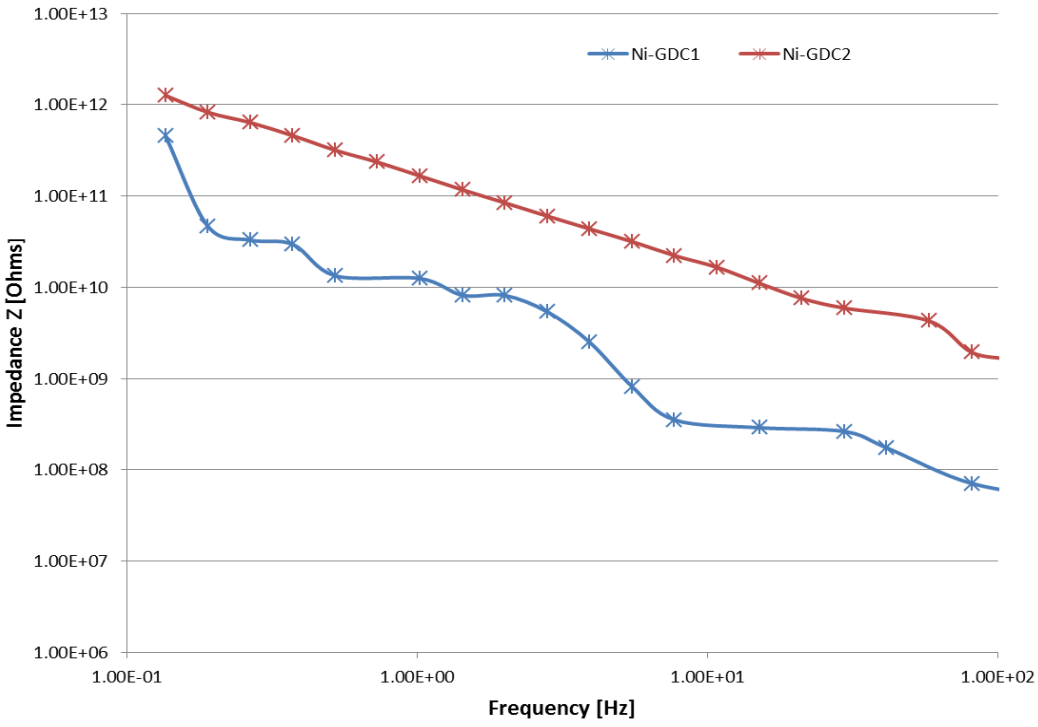

Figure 2.8. Ni-GDC1 and Ni-GDC2 frequency dependent impedance results.

When examining the Ni-YSZ samples we clearly see that the sample with higher porosity and larger pore width at the surface has given a higher conductivity. However, when examining the Ni-GDC samples we see that the sample porosity for both Ni-GDC1 and Ni-GDC2 is fairly high and in both cases you also see a cone shaped microstructure. The difference here is that Ni-GDC1 has an overall larger average pore size than Ni-GDC2 and as seen from the plot this resulted in lower impedance results. Therefore we can determine that not only porosity but also pore size can be an important characteristic when trying to obtain the ideal conductivity for a SOFC.

2.4 CHAPTER SUMMARY

In this chapter we have demonstrated that solid oxide fuel cell (SOFC) materials can be characterized based on their porosity, pore shape and pore size using 3D X-ray microscopy and subsequent image processing. We have then seen that we can use broadband dielectric spectroscopy to relate these characteristics to dielectric properties of our ceramic materials. BbDS is proven to be an effective method of capturing changes in dielectric characteristics due to microscopic changes in SOFC materials. Results show that porosity and pore size, as well as, pore shape are important contributors to manufactured material properties. This information can be useful for a number of reasons. Results of image analysis can be used efficiently as input in multi-scale modeling of SOFC anodes. This will enable us to better predict solid oxide fuel cell behavior and to accurately design a porous microstructure tailored to our needs. More parametric studies with porous geometric design and different material system may be investigated in the future.

CHAPTER 3

MATERIAL STATE DESCRIPTION OF DAMAGE DUE TO LOW VELOCITY IMPACT AND EVOLUTION OF REMAINING PROPERTIES OF COMPOSITE MATERIALS

3.1 BACKGROUND

If an external object strikes the surface of a composite structure it can damage the structure and degrade the load bearing capabilities of the structure [14]. Generally, a low velocity impact may not show externally visible damage but can cause significant internal damage. Such internal damage from impact event may grow with time (for example, cyclic loading) and could eventually lead to a global failure of the composite structure [15]. There have been a number of studies on residual strength and fatigue characteristics of composite materials that have been subject to impact damage and a number of models have been developed. Caprino [16] developed a simplistic model to predict the residual strength after impact; where tensile and residual strength is related to incident impact energy and threshold impact energy. Davies et al. [17] found that the residual strength of a composite material is rapidly reduced as damage area due to impact increases, and they report that the relationship between the residual compressive strength and impact energy approaches an asymptote. There have also been a number of models created to predict residual strength in which the damage area is replaced with a hole. [15]. Koo et al. [18] concluded that the residual strength after impact can be estimated by measuring the size of the permanent impression on the surface of the composite.

While the above models and conclusions may give us useful information regarding residual strength of composite materials after impact, many of them require knowledge of the impactor size, the impact energy or the damage area to be effective. This is a serious issue when considering damage caused by low velocity impact. It is more often that in practical applications the impact energy on the composite structures will be unknown. Determining damage area due to barely visible impact and corresponding remaining property can be a challenging problem. Performing any kind of destructive test to determine mechanical properties after impact would also be extremely impractical.

There is a need for a non-destructive method to relate changes in microstructure due to impact damage to residual mechanical properties of composite structures and have a prognosis of durability. These non-destructive methods must be practical, while maintaining accuracy when evaluating material state change. It is also important to determine when damage within the material may be interacting. Ultimately, the ability to predict mechanical property degradation due to unseen damage within a composite structure is a challenging problem.

As discussed in the introduction (1.2.1), there are several initial interfaces or heterogeneous material boundaries in the composite materials. However, as damage is induced, many new interfaces begin to develop within the material. Each of these interfaces or material boundaries now becomes a new location of charge accumulation. The measured permittivity of a composite can be considered a state variable that is determined by how the composite is designed and manufactured initially, and by the changes that occur in material state as defects develop. Prior work by Prof. Reifsnider

and Dr. Majumdar's groups has demonstrated that dielectric properties of woven glass fiber composite materials measured using BbDS can be directly related to the remaining mechanical properties of the material subjected to end-loaded bending [35-38].

The objective of this chapter is to use BbDS to determine the material state change in a composite that has been subject to low velocity impact damage. The dielectric properties of the material will then become material variables and depend on applied impact energy. Finally, the dielectric variables will be related to mechanical properties such as residual strength and stiffness of composite material.

3.2 EXPERIMENTAL PROCEDURE

3.2.1 Specimens of different material type and Impact test procedures

In this experiment we will look at three different cases. In the first case, we will examine a 1mm thick, 45 degree woven glass fiber reinforced composite material. In the second case, we will examine a 3mm thick quasi-isotropic carbon fiber polymer reinforced composite material and finally we will take a look at a case where a 0.6mm thick cross-ply carbon fiber composite material is used. In each case damage is induced using the impact tester with hemi-spherical impactor (Figure 3.1). For the glass fiber and cross-ply specimens a 2lb impactor is used; however for the quasi-isotropic carbon fiber material a 4lb impactor is used to induce damage. In all cases the impactor has a tip diameter of half inch. The energy levels used are dependent on the specimen type. The 1mm glass fiber specimens were impacted at four different energy levels: 1.3J, 1.8J, 2.7J and 3.6J. The quasi-isotropic carbon fiber specimens were impacted at 3 different energy levels below the BVID region. Upon careful observation it was determined that BVID was below 18J, therefore the impact energies selected were 14.5J, 16J and 18J. The cross-

ply carbon fiber specimens were subject to 6 different impact energies 2J, 3J, 4J, 5J, 6J, and 7J to sequentially show the increase in damage within the specimen.

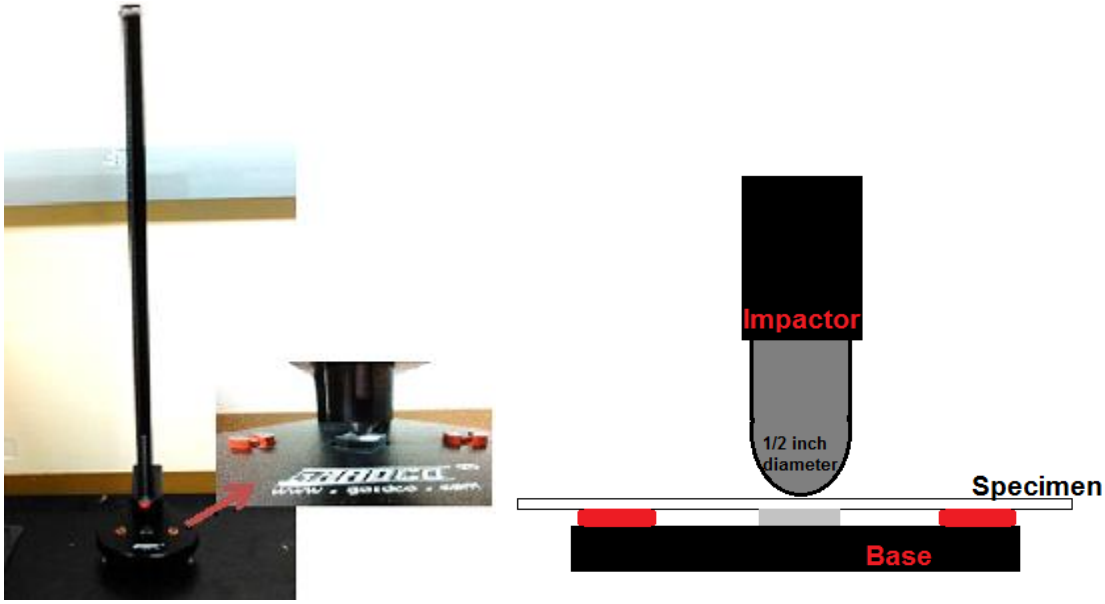

Figure 3.1. Standard impact tester used for low velocity impact.

3.2.2 Mechanical Testing Procedures

In addition to dielectric measurements, our carbon fiber specimens are also subject to mechanical tests. Modulus tests have been conducted on each carbon fiber sample to highlight the modulus degradation as the samples are subject to impact and allow us to compare these findings to change is dielectric response. Secondly, once all other testing is complete the cross-ply carbon fiber specimens are pulled to failure to determine ultimate tensile strength (UTS). This will give us yet another material variable to compare to the dielectric material variables we have previously found. All mechanical tests have been done using standard universal testing machine (MTS Landmark).

3.2.3 Dielectric measurement procedures

Dielectric measurements of each sample have been taken before and after impact on every sample using the same Novocontrol BbDS equipment described in chapter 2, however the built-in thermal chamber is not used in this case. Instead, a customized design of a specimen holder with copper electrodes has been developed to mount the samples and is connected to the BbDS unit. This bulk scanning mode uses two-inch by half-inch electrodes on either side of the specimen to scan the entire potential damaged area.

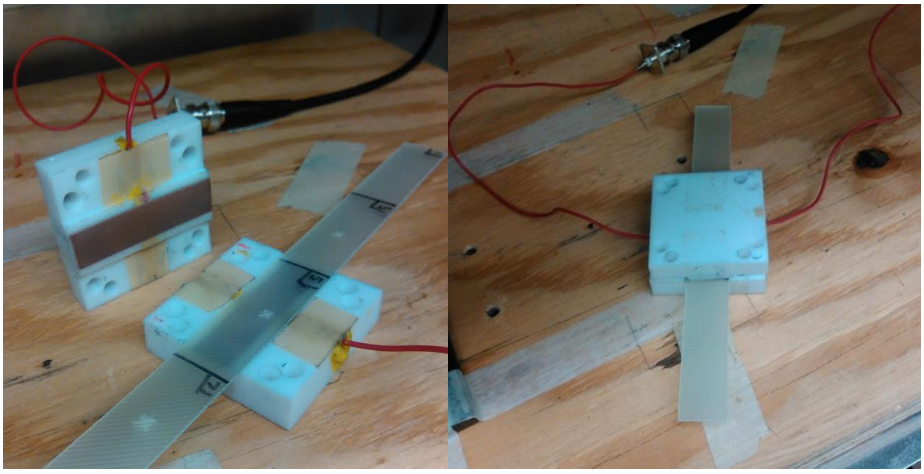

Figure 3.2. Glass fiber specimen in electrode assembly for bulk BbDS

3.2.4 Visualization Methods

After the BbDS measurements have been taken, the next step is to analyze the damage that has been caused by the impact so that we can relate this damage to the change in dielectric properties. For the glass fiber specimens we use a red dye to highlight the matrix cracking and delamination that has occurred, then we examine the specimen using a digital microscope. The microscope used is a QX500 smart and

precision digital microscope with 5X to 500X magnification capabilities. Images of the damage are then taken using the built in microscope software and the damage area is approximated used a built in measurement tool.

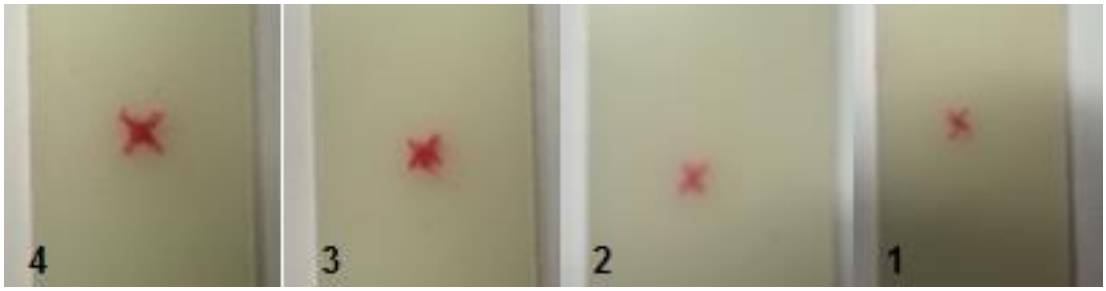

Figure 3.3. Damage area in Glass fiber specimens subject to low velocity impact damage

Damage in the carbon-fiber specimens (both cross-ply and quasi-isotropic) is analyzed using the 3D-Xray microscope that was previously described in Chapter 2. Images of the microstructure are taken at 4X magnification to allow us to see through the entire thickness of the specimen and higher magnifications may be used for understanding very local damage features.

3.3 RESULTS AND DISCUSSION

3.3.1 Glass-Fiber subject to impact damage bulk measurement results

Details about experimental parameters (specimen, drop height or impact energy levels and approximate damage area) for our four glass fiber specimens are summarized in the Table 3.1 below.

Table 3.1. Glass-fiber/Epoxy composite impact energy and damage Area

Specimen No	Drop Height *(m)*	Impact Energy *(J)*	Approximate Damage Area ($\boldsymbol{mm^2}$)
1	0.15	1.3	0.9

2	0.2	1.8	1.92
3	0.3	2.7	3.92
4	0.4	3.6	5.6

We can then plot these results and determine that at these low impact energy levels, the damage area and the impact area have a linear relationship. This kind of trend is important to note as it can assist us with modeling the effects of impact on a particular material type. Below is a plot of the approximate delamination area developed due to different impact energies for our off-axis (45 degree) woven glass fiber, epoxy composite material.

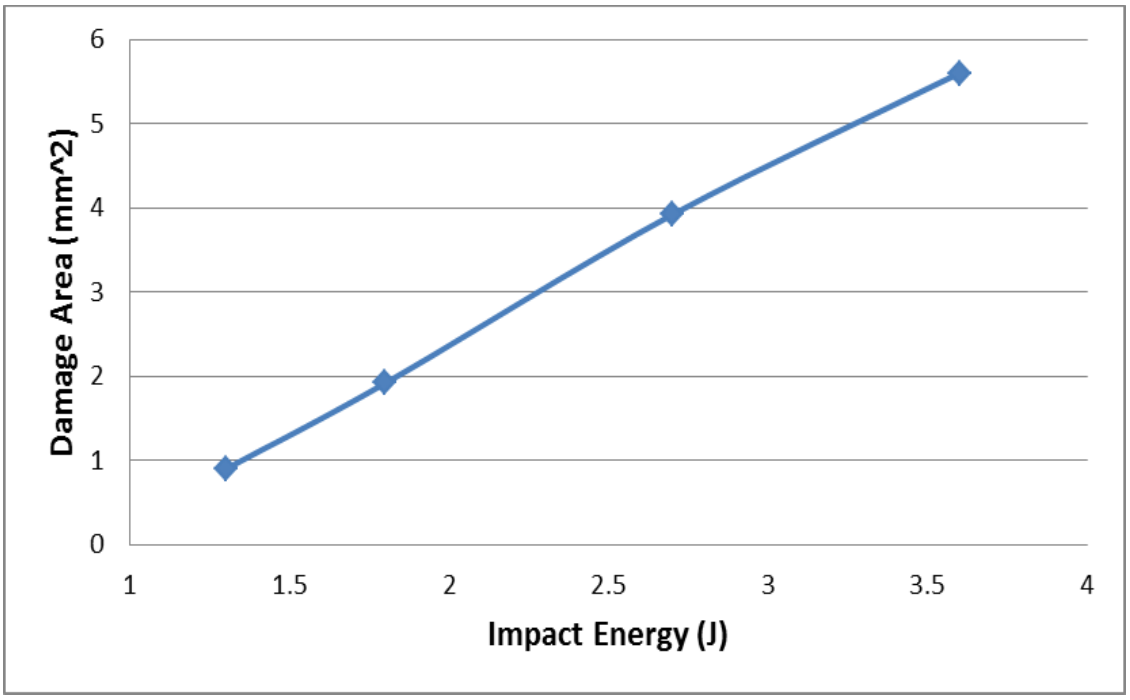

Figure 3.4. Damage area of glass fiber specimens as a function of impact energy.

While examining our bulk BbDS results for the four glass fiber specimens subject to a single impact, it is important to remember that the dielectric response of our material can be seen as a material property. In this case we will look at impedance change in our material as a function of both the impact energy induced and the resulting delamination area.

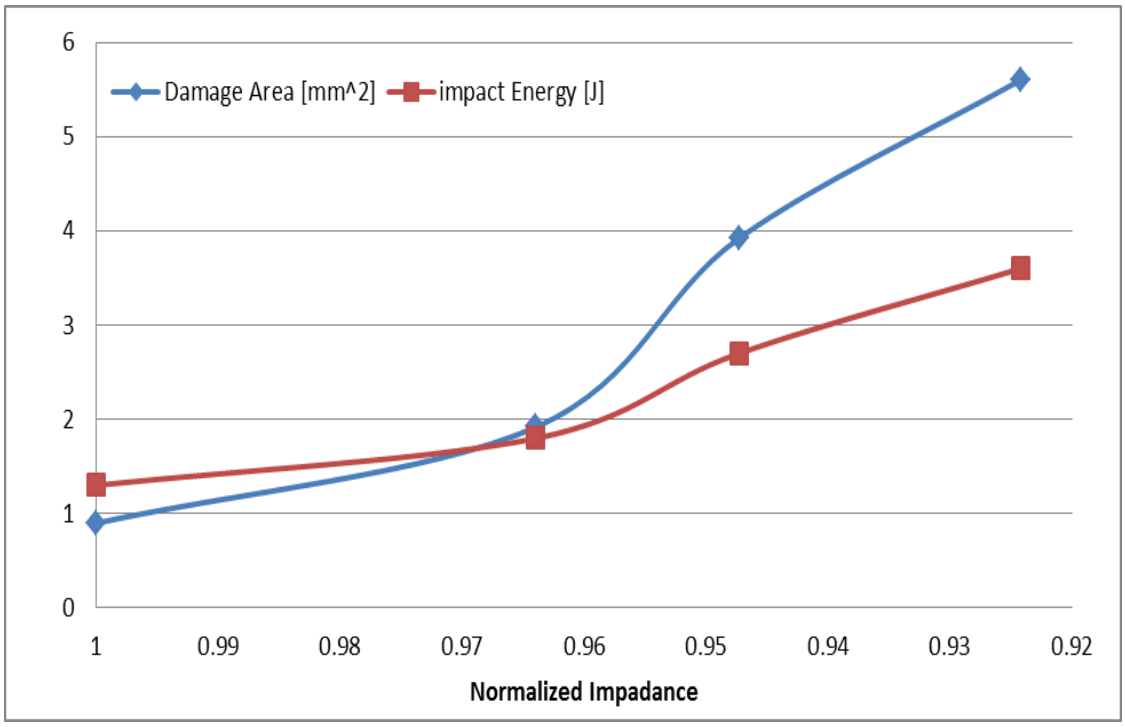

Figure 3.5. Change in Normalized impedance at 0.1Hz as a function of delamination area and impact energy

3.3.3 Barely visible impact damage results on a quasi-isotropic carbon fiber composite

For our quasi-isotropic specimens we have taken bulk BbDS measurements and looked at change in complex permittivity of our four samples damaged in one location at four different energy levels. As seen from figure 3.6, there is a large change in both real and imaginary permittivity between the 16J and 18J impact energies. From this we can determine that there is significantly more damage present in the 18J specimen and even a large delamination area.

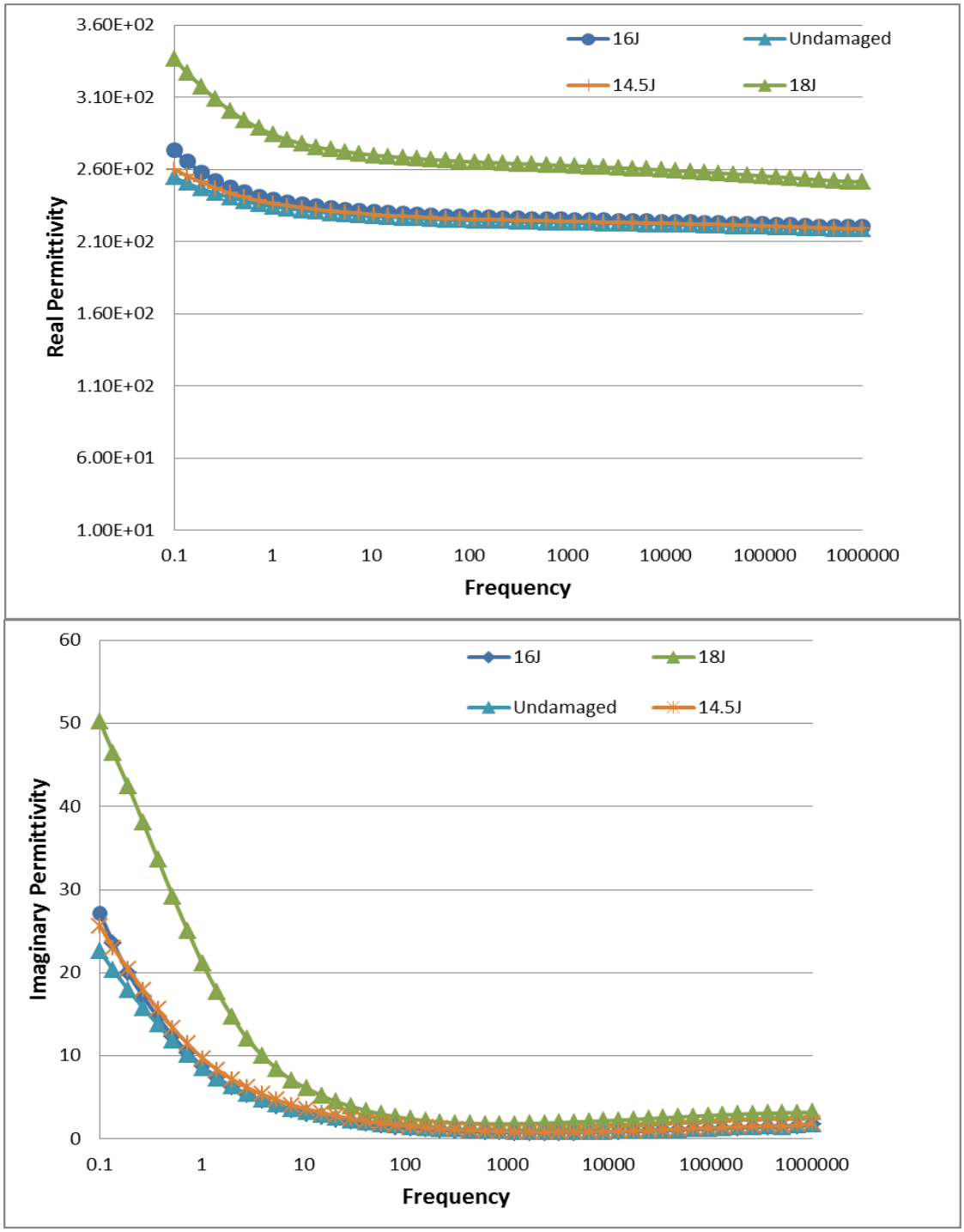

Figure 3.6. Complex permittivity as a function of frequency with increasing impact energies

We have taken x-ray images at these two different energy levels to visualize what is going on as a result of this large change in dielectric properties.

Figure 3.7. 3D X-ray images (4X magnification) of quasi-isotropic carbon fiber specimens impacted at 16J (above) and 18J (below)

We will also compare the changes in permittivity to modulus data for three damaged specimens and one undamaged specimen. Figure 3.8 clearly demonstrates that the changes in imaginary permittivity are more sensitive to the impact damage than the changes in modulus. Where we see little to no change in modulus there is a definite change in permittivity of the material.

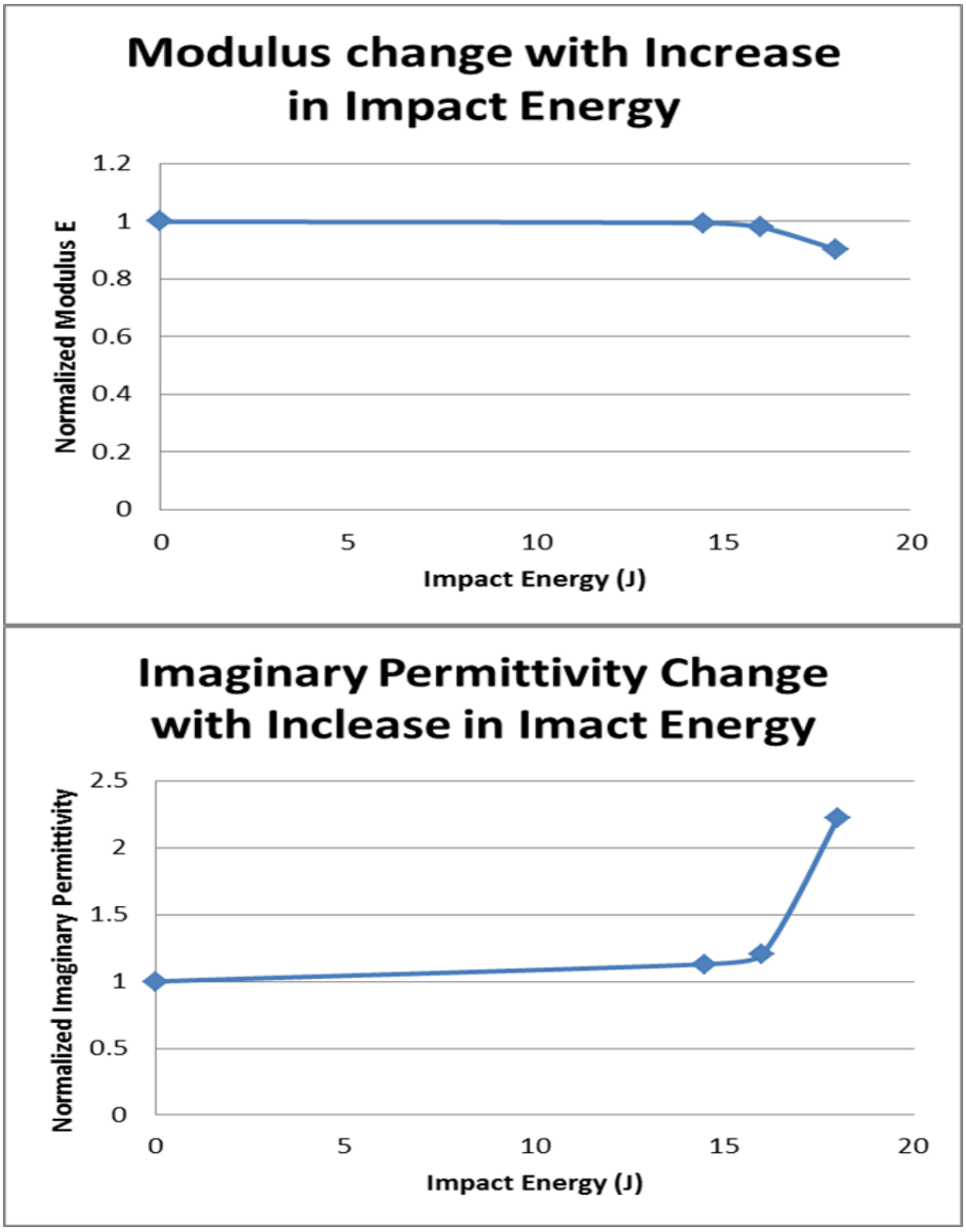

Figure 3.8. Normalized modulus and imaginary permittivity data as a function of impact energy.

3.3.4 Low velocity impact damage results on cross-ply carbon fiber composite specimens

For the cross-ply specimens we have taken dielectric results using BbDS. We will be considering the frequency dependent change in real permittivity with microstructural changes due to low velocity impact damage.

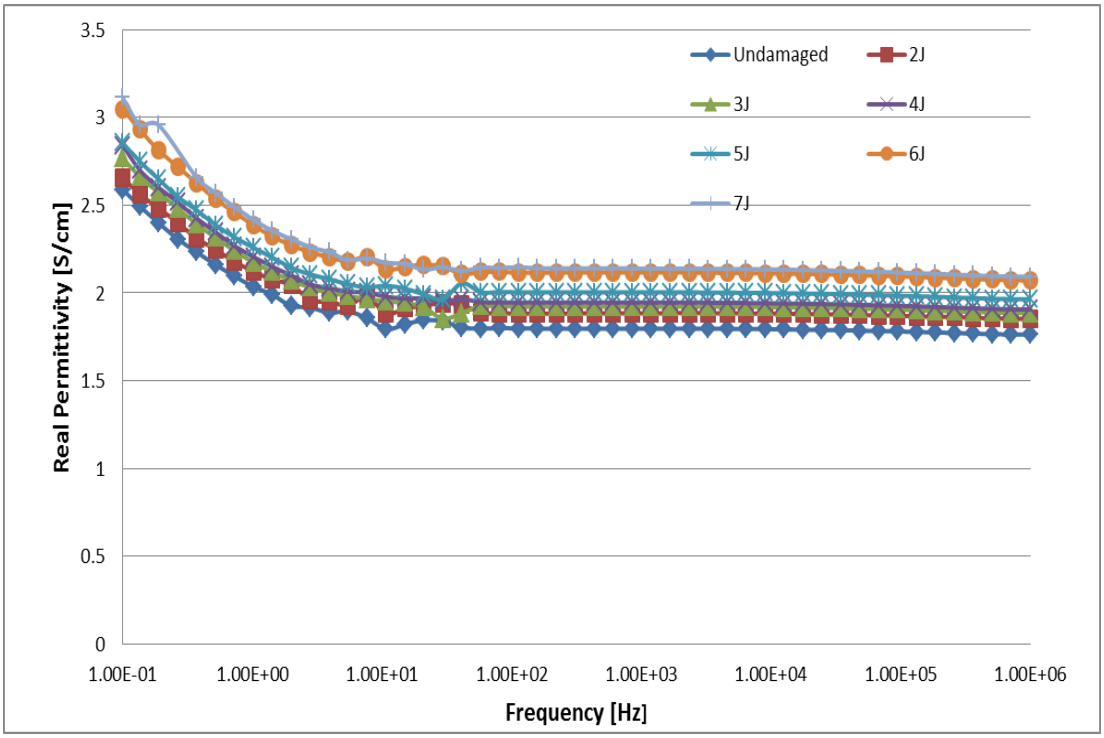

Figure 3.9. Change in frequency dependent real permittivity of cross-ply Carbon fiber specimens as impact energy increases

From these results we can see that material state change due to impact is being captured by the change in real permittivity response. To ensure material state is changing and validate our results we would like to visualize these changes.

Surface images of the impacted specimens (on the side opposite to impact) show a fracture path present on impacted samples ranging from 3J to 7J. As expected this fracture path is increasing in both length and thickness as the impact energy increases. With this in mind we can take a look at the impacted microstructure throughout the specimen using 3D X-ray microscopy. Our 3D images show that damage is also present in the 90 degree layers of our specimens that have been subject to 3J to 7J impact energies.

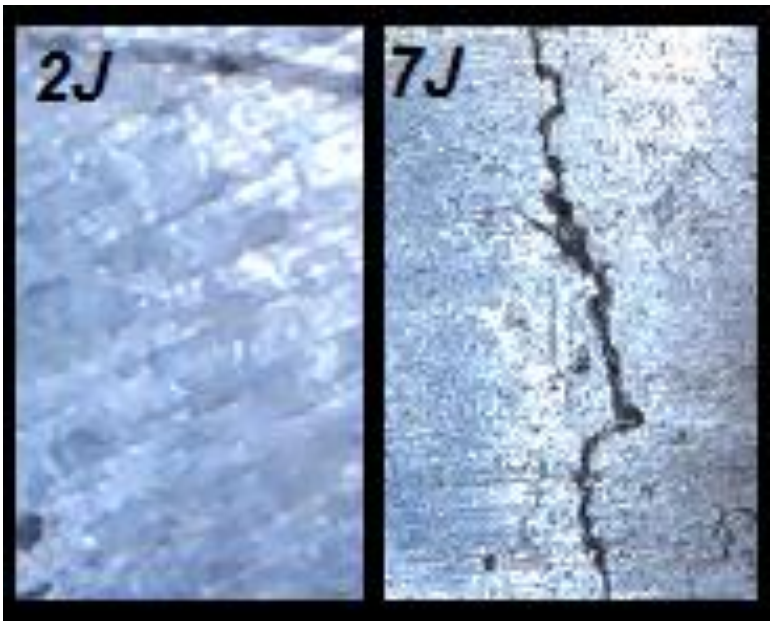

Figure 3.10. Comparison between 2J and 7J impacted specimens (image taken on the opposite side of impact)

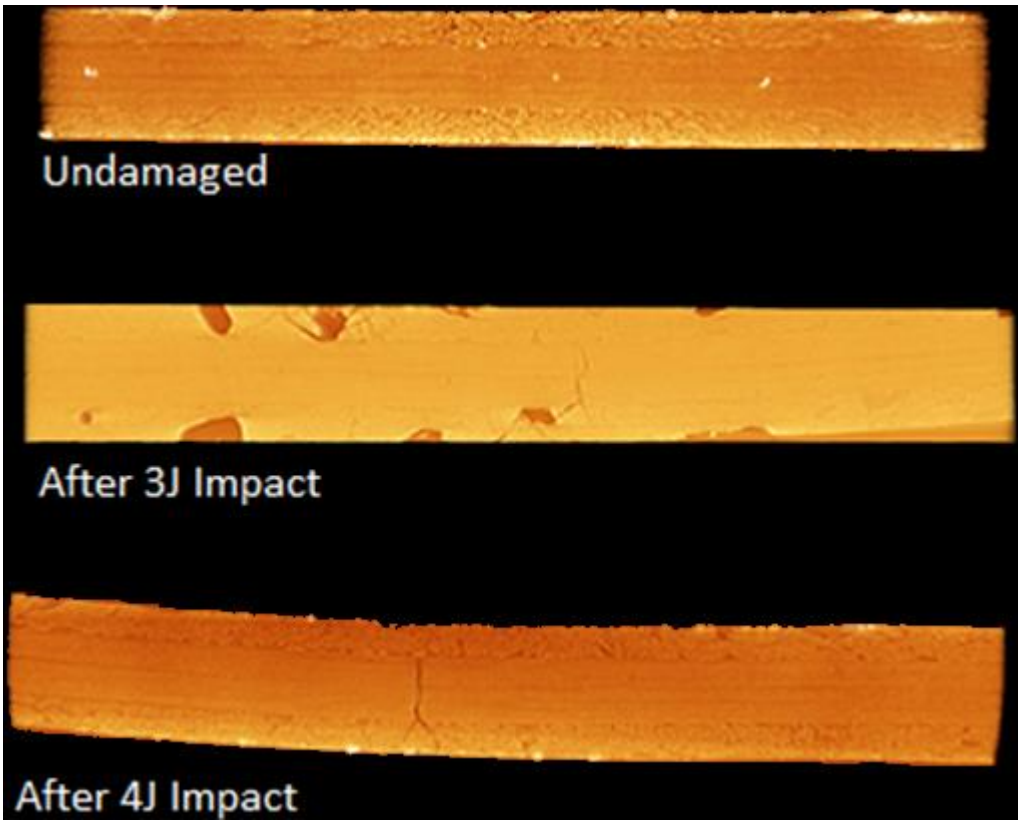

Figure 3.11. X-ray images of undamaged and damaged Cross-ply specimens.

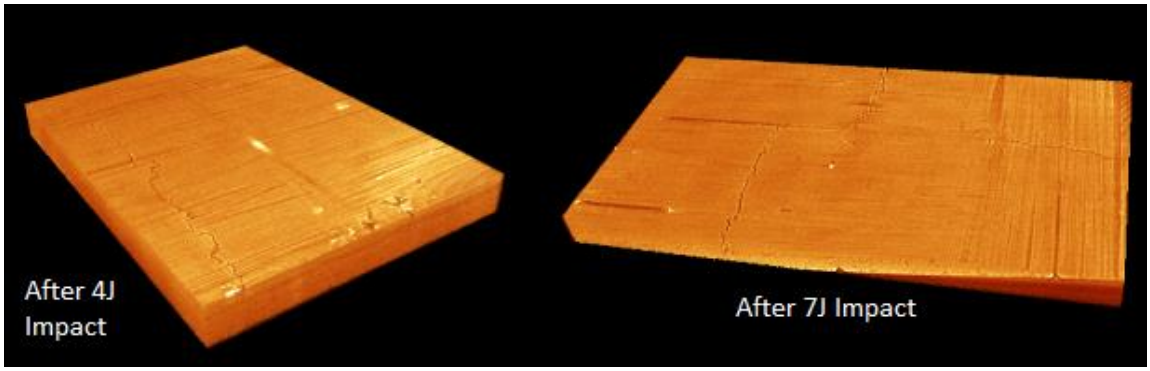

Figure 3.12. 3D X-ray images of specimen after a 4J and a 7J impact.

We would now like to relate our dielectric property variables to changes in mechanical properties of our specimens. In this case study we will relate our results for our change in real permittivity at a set frequency (0.1Hz) to the change in modulus as well as, the change in ultimate tensile strength (UTS) of our specimens.

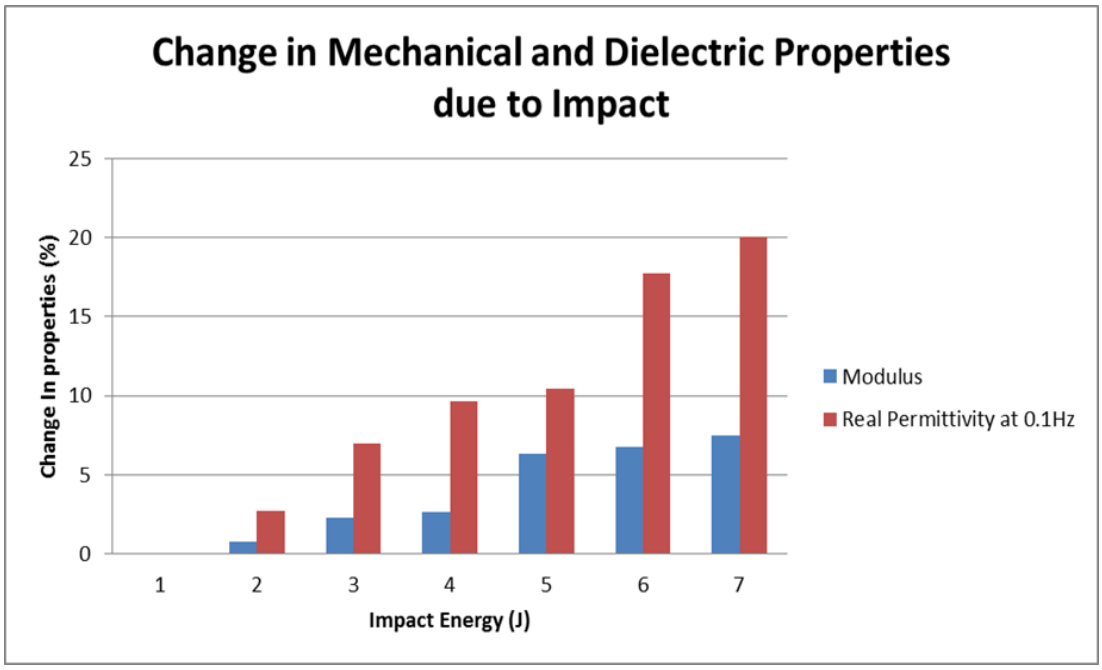

Figure 3.13. Percent Change in real permittivity and modulus with increasing impact energies

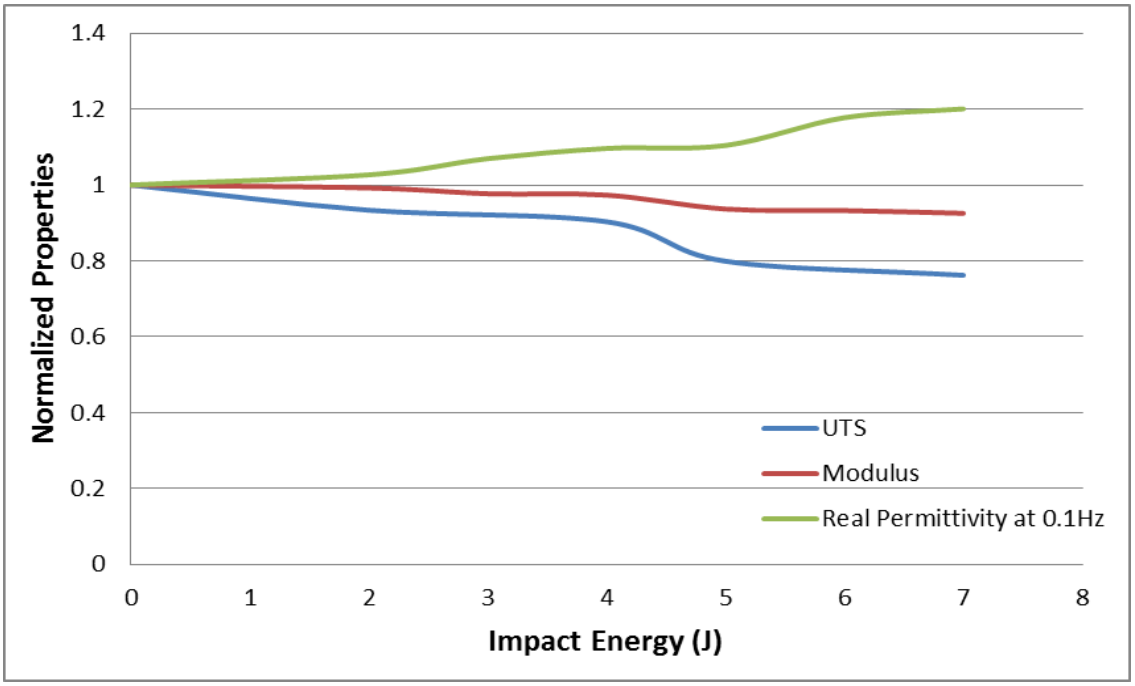

Figure 3.14. Change in normalized properties in cross-ply specimens subject to impact damage.

3.4 MODELING FRAMEWORK

Dielectric variables can be used alongside mechanical data of our specimens subject to low velocity impact damage to create a modeling framework for a specific material type. We can use a simple power law expression to show that degradation laws can be written using material variables. Here we have used a power law expression to show that the change in modulus of our cross-ply carbon fiber specimens can be predicted by examining changes in real permittivity.

$$\Delta E = A(\Delta \varepsilon')^{j}$$

Here *j* and A are material parameters. Here we have used a simple curve fit to determine *j* =0.1.2 and A=2. In future work, an estimate for such parameters can be achieved with more theoretical formulation of dielectric properties as well as validation experiments.

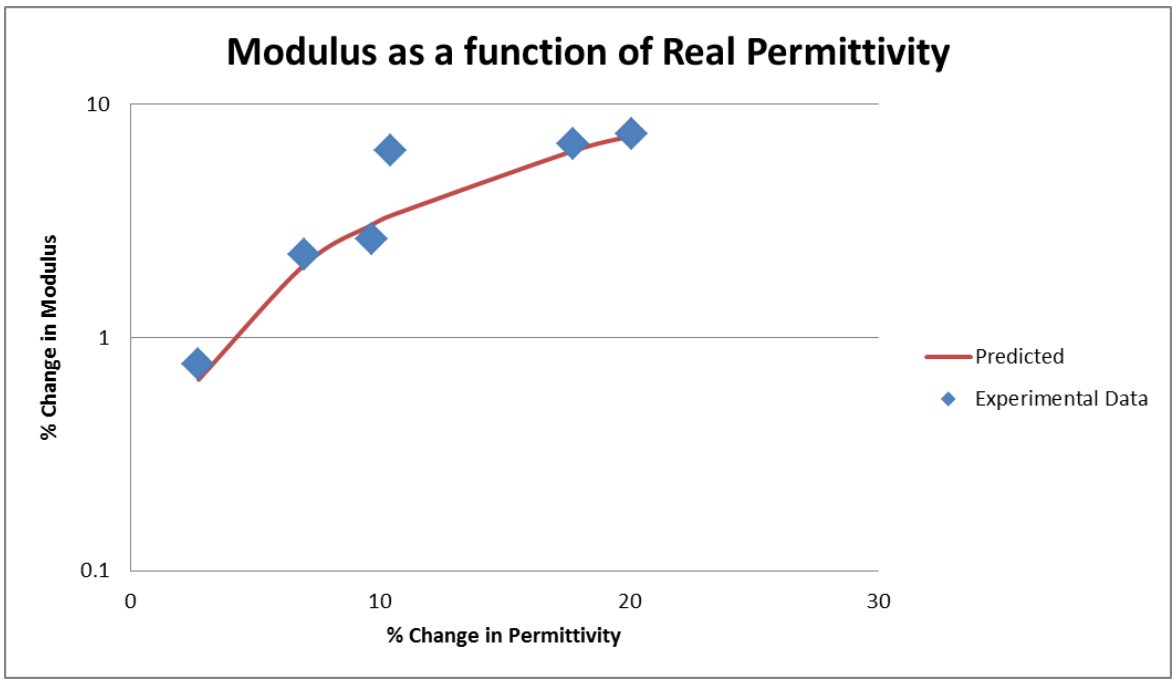

Figure 3.15. Predicted modulus degradation in cross-ply specimens as real permittivity is increasing due to impact loading

It is possible to calculate dielectric properties from geometry or estimate of damage area. For delamination modeling if we take delamination area and assume it to be a sphere or randomly oriented ellipsoid we can use the following equation from Kremer's [19] to calculate the resulting dielectric constant. The following equation is to be used when you have a heterogeneous material, where both parts have complex permittivity.

$$\varepsilon_c^*(\omega)^{\frac{1}{3}} = \varphi_1\varepsilon_1^*(\omega)^{\frac{1}{3}} + \varphi_2\varepsilon_2^*(\omega)^{\frac{1}{3}}$$

Where ε_c^* indicated both real and imaginary portions of the resulting complex permittivity. φ is the volume fraction of the component and ω is the radial frequency.

$$\varepsilon^* = \varepsilon' - i\varepsilon''$$

Here we see that the resulting complex permittivity is a simple function of the complex permittivity of both components within the medium. In the simplest form we can use this equation to determine our resulting permittivity for a composite material. When we consider the material itself to have a constant permittivity and the defects to have the permittivity of air in a vacuum, we say that $\varepsilon_2^* = \varepsilon_0^*$. If the permittivity of both the damaged and undamaged specimens is known by using broadband dielectric spectroscopy, a simplistic calculation can then be used for approximate delamination volume prediction.

$$\varphi_2 = \left(\frac{\varepsilon_c^* - \varepsilon_1^*(\omega)^{\frac{1}{3}}}{\varepsilon_1^*(\omega)^{\frac{1}{3}} - \varepsilon_0^*(\omega)^{\frac{1}{3}}} \right)$$

More complexity can be added to such simplistic model as needed. Alternately, a RVE based micromechanics scheme can be solved computationally using Finite element method. The advantage here is that dielectric properties of constituents are known from our experiments and we can use those for future micromechanical model.

3.5 CHAPTER SUMMARY

In this chapter we have demonstrated a new technique for capturing the changes in material state due to impact damage. Using broadband dielectric spectroscopy we can assign new dielectric material variables to our specimens. We can then relate these dielectric results to changes in mechanical properties due to impact. The advantage of this technique is that now we are able to use our dielectric data to predict changes in

mechanical properties of a composite structure when impact energy and damage area are unknown. This will allow for new models to be developed using these material relations. We have demonstrated a preliminary framework for predictive models using dielectric variables, more complexity can be added to these models for use in a wide variety of application.

CHAPTER 4

EVOLUTION OF DAMAGE: LOCAL MECHANISMS AND DISTRIBUTION OF PROPERTIES

4.1 BACKGROUND

As composite materials become increasingly popular in a number of different fields it is important to understand exactly what is occurring inside the material. The evolution of damage over time within a composite material is complex. Not only would we like to know if there is damage present, but we would also like to know the exact location, modes, and property loss associated with it. This kind of information will aid us to understand damage growth and interaction possibilities which will govern durability.

With knowledge of the damage evolution process, it is clear that a reliable means of material state prediction is critical for the utilization of composite materials. Kessler et al. [20] presented an experimental and analytical survey of candidate methods for in-situ damage detection within composite materials. In Kessler's work a laser vibrometer was used to capture changes in natural frequencies and relate them to damage modes. Kessler also created 2-D finite element models that accurately predicted the response of the specimens at low frequencies, but was unable to detect mode-dependent damage evolution at higher frequencies. Zou at al. [21] presented a review of vibration-based techniques that are dependent on models for identification of delamination in composite structures. In this work, model-dependent methods use piezo sensor and actuators along with finite element analysis results to locate and estimate damage events by comparing

changes in dynamic responses. These model-dependent methods are shown to be capable of providing both global and local damage information. The authors admit however, that the downfall to these model analysis methods is that they lack the ability to detect very small damage and they require large data storage capacity for comparisons. Valdes et al [22] used piezoceramic patches and piezoelectric film sensors to detect delamination in composite materials, without the use of models. Frequency sweeps (8 to 14 kHz) were used to induce vibrations on the structure; reductions in models frequencies were found as the delamination area in the specimens were increased.

We have shown that we can capture increasing damage within a material by examining material state changes through the use of broadband dielectric spectroscopy, now the focus is determining how the dielectric data relates to different local events such as damages modes within the material. We would also like to determine if we can predict not only the location of the damage but also distribution of remaining properties over that localized damage volume. This is not reported in the literature on fiber reinforced composite materials. The objective of this chapter is to capture damage location controlled spatial influence zone of interaction which leads to property variation within a composite specimen, while linking dielectric signatures to certain damage modes.

4.2 EXPERIEMENTAL PROCEDURE

Three different test cases will be presented. In the first test case, BbDS measurements are taken using a moving line scanning method to determine dielectric properties as a function of position along the specimen. In the second test case we will simulate delamination in our specimen at three different locations and examine the change in through-thickness BbDS response at different delamination locations to to

demonstrate that bulk BbDS measurements are not simply volume fraction effect but sensitive to location also. Finally, in the third case, specimens will be subject to static tension tests at different loading levels and the change in BbDS response will be examined at different intervals upon unloading. This may help capture transition of damage mode (for example, matrix cracking, delamination and finally fiber fracture) as the specimen is progressively loaded to failure.

4.2.1 New Scanning BbDS (Line Scanning) Method

A glass fiber specimen is subject to impact damage at two different locations along the specimen, the damage energies are 3J and 5J respectively. Damage mapping will be performed on this specimen using the Novocontrol broadband dielectric spectroscopy unit. In this case measurements are taken using a cylindrical electrode on one side and a base electrode on the other.

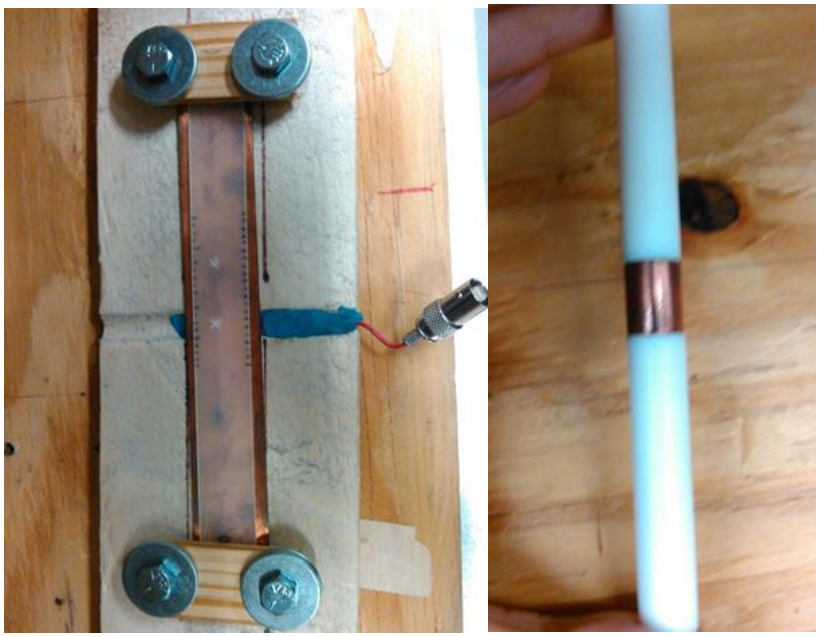

Figure 4.1. Cylindrical roller electrode (right) and base electrode with glass fiber specimen in place for moving line scanning BbDS testing.

A moving line scan is performed by securing the specimen on the base electrode and moving the cylindrical electrode along the specimen at a constant rate. BbDS measurements are then taken at a constant frequency (10Hz) over a set amount of time. The measurements as a function of time were then related to distance along the specimen depending on the scanning velocity.

4.2.2 Damage Location Sensitivity of Dielectric Properties

Four carbon fiber reinforced composite specimens are fabricated. One of the specimens is undamaged and the other three have a 1mm by 1mm piece of Teflon tape implemented at different locations within the specimen to simulate delamination. The specimen layup and delamination locations can be seen in figure 4.2.

Figure 4.2. Specimen layup and planned delamination locations.

Dielectric measurements were then taken on each of these specimens using the BbDS test setup described in chapter 3 and the same two inch by half inch bulk copper electrodes. Although the same size of delamination is present over the entire volume, the dielectric property data clearly shows sensitivity to delamination location in those controlled specimens. Hence it is understood that BbDS measurements provide property

estimates based on actual material configuration over the volume and hence captures their interactive response within the discrete volume of observation.

4.2.3 Quasi-Static Tensile Loading and BbDS Property Evolution

Three different carbon fiber reinforced specimens are fabricated each with 8 plies: a unidirectional sample, a cross-ply samples and a quasi-isotropic sample. Each of these specimens are subject to different levels of static tension loading induced by a MTS machine.

Figure 4.3. MTS machine with cross-ply specimen and extensometer

Samples are unloaded at different levels of load and broadband dielectric spectroscopy data is taken after each unloading. The change in BbDS response is observed as the samples are loaded closer and closer to ultimate tensile failure. Because

each specimen has a different fiber layup they will go through different damage modes at different loadings throughout the testing. We can then determine the difference in dielectric response patterns for each specimen. We will then visualize and validate these damages modes using 3D X-ray microscopy.

4.3 RESULTS AND DISCUSSIONS

4.3.1 Mapping of BbDS Properties over Damaged Volume

Here we can see the change is real permittivity at 10Hz as a function of distance along the specimen (Figure 4.4).

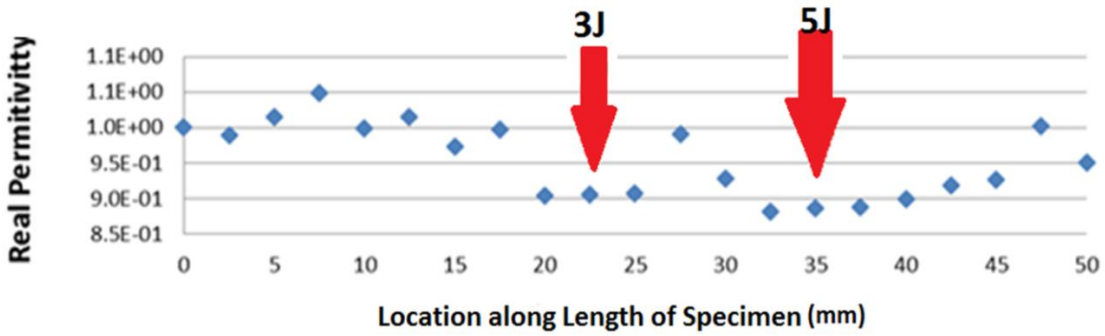

Figure 4.4. Real permittivity of a glass fiber specimen subject to impact damage as a function of location along the specimen.

This delamination mapping technique is useful for a number of reasons; one being that we are now able to capture the interaction between the damage sites. As seen from the plot, between the two damaged locations the real permittivity does not return to the initial real permittivity captured at the end of the specimen. We can also see exactly where is the specimen the damage begins to be present, this will greatly aid in determining exactly how large of an area has been affected by this impact. The unique contribution is that we now have a local property variation in terms of material variable

and this can be predicted. Moreover, as discussed in earlier chapters, dielectric property has been related to remaining mechanical property and a similar correlation can be established to get local variation mechanical properties too. More work needs to be done but these preliminary observations certainly provide a path way in that direction.

We can also note that this method has a great potential to be adopted for various industry applications. If a roller system similar to this one is put in place it could be practically used for determining defect and property distribution during manufacturing layup.

4.3.2 Damage Location Sensitivity of Dielectric Properties

Results show that the dielectric response of the carbon fiber reinforced composite material is dependent on the delamination location. From figure 4.5 we can see that at location two the permittivity response is significantly higher. Interestingly, we can clearly see that the location is much more sensitive when examining real permittivity and this is consistent with the fact that capacitance contributes to real permittivity. This information can help us to better understand the dielectric responses we may encounter when examining an impacted specimen that may be subject to delamination due to impact. Delamination clearly creates new surfaces which are separate by a distance and hence contributes to capacitance of material.

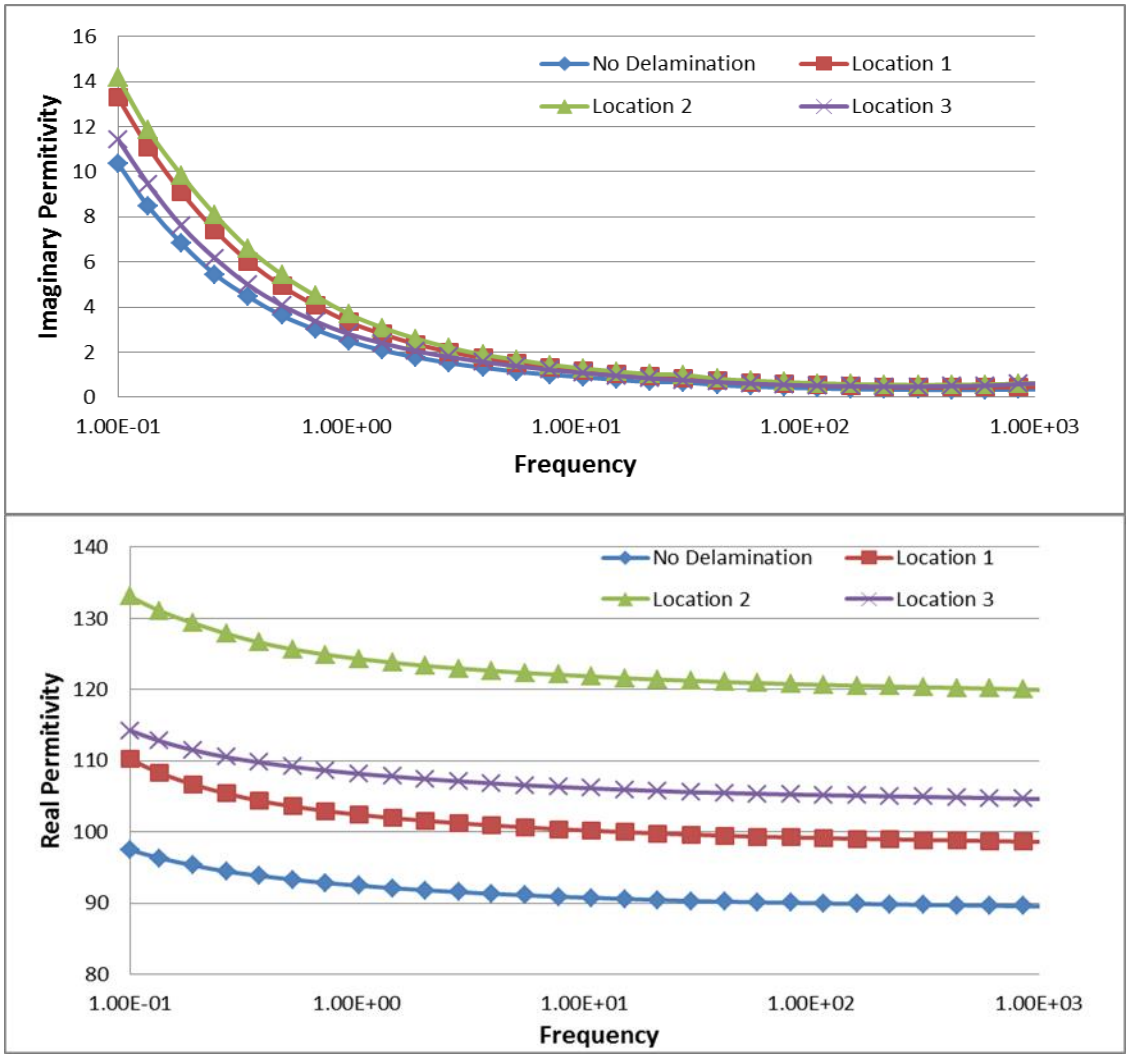

Figure 4.5. Change in complex Permittivity as a function of frequency at different delamination locations.

4.3.3 Evolution of Damage and Corresponding BbDS Property Signatures

As we relate our BbDS results for each specimen subject to different tensile loadings we can see differences in BbDS response to predicted damage mode. For the unidirectional specimen we expect to see significant fiber breaks to occur, however for the cross-ply specimen we expect to see significant matrix damage before fiber breaks dominate the response prior to failure. The dielectric results for these two specimens are compared in figures 4.6 and 4.7 below.

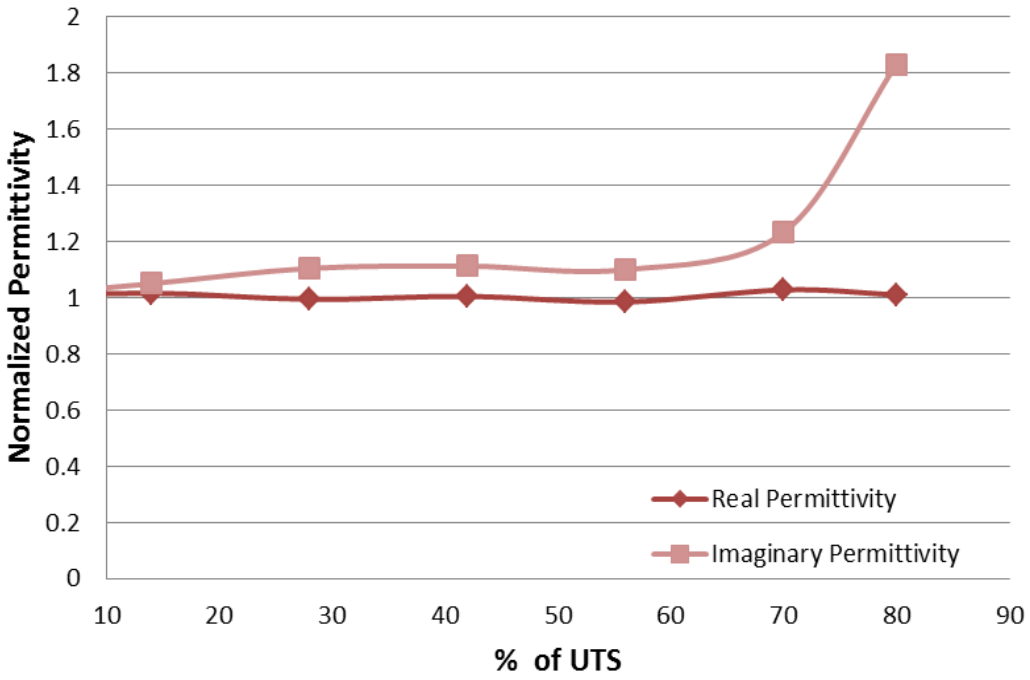

Figure 4.6. Change in permittivity at 0.1Hz with increase in tensile loading for Unidirectional specimens.

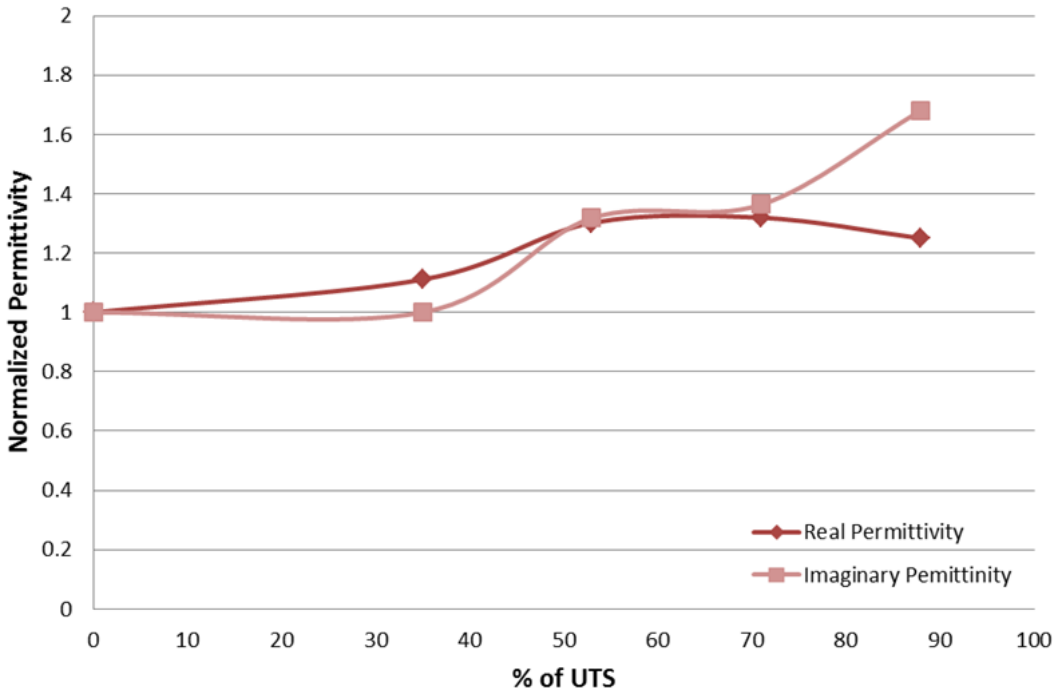

Figure 4.7. Change in permittivity at 0.1Hz with increase in tensile loading for Cross-ply specimens.

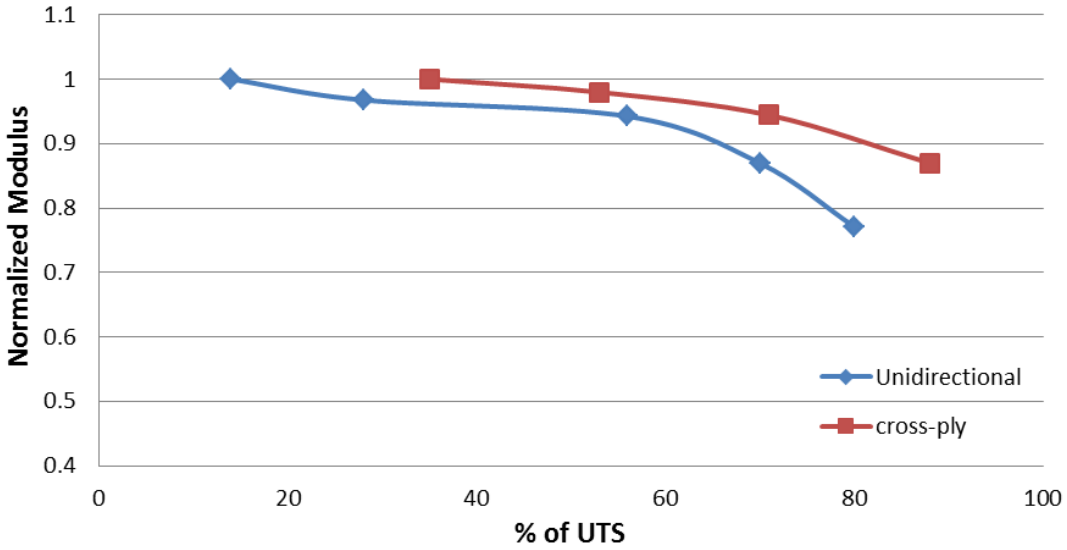

Figure 4.8. Change in Modulus data of unidirectional and cross-ply specimens as applied tensile force approaches UTS

We can validate these results through 3D X-ray microcopy images. By examining the microstructure of the uni-directional specimen we can see that packets of fiber breaks have occurred after the 17200N tensile force was induced. In comparison we can see that in our cross-ply specimen we see matrix cracks after 12000N and broken fibers at 15000N.

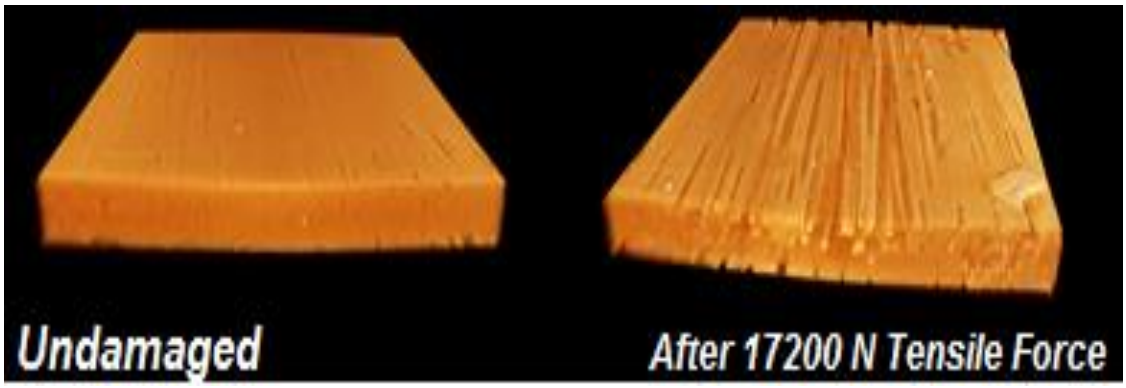

Figure 4.9. 1X 3D X-ray images of 8ply unidirectional Specimens: Undamaged and after 17200N Tensile Force

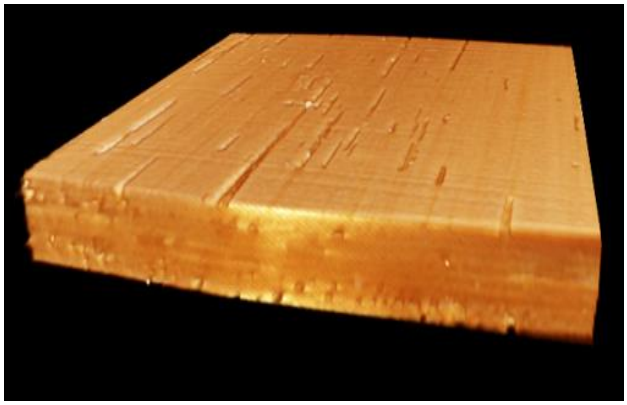

Figure 4.10 1X 3D-Xray Image of cross-ply specimen subject to 12000N tensile force

From the above images we can see that the microstructure has dramatically changed from when the specimen was subjected to 12000N to when the specimen was subjected to 15000N. Therefore we can confirm that the dramatic change in imaginary permittivity between these two tensile forces was due to fiber breaks. However, if we take a closer look at the specimen when it was subject to 12000N we can see that matrix damage has developed inside the specimen after this leading. We can now see that the changes in microstructure due to matrix damage were captured by both the real and imaginary parts of permittivity. Interestingly, we see that the real part of permittivity was more sensitive to the initial matrix cracks being formed inside the specimen.

Figure 4.11. 4X 3D X-ray image of cross-ply specimen subject to 12000N tensile force (Matrix Damage present)

Figure 4.12. 1X 3D X-ray Image of cross-ply specimen subject to a 15000N Tensile Force

We can clearly see an increase in the damage due to tensile loading in the 15000N cross-ply specimen as opposed to the 12000N specimen. If we compare this damage to our results we see that the broken fibers present have been captured by a sharp increase in imaginary permittivity as opposed to real permittivity that was increasing at a constant rate when matrix damage was beginning to appear. This confirms that our BbDS results are dependent on damage modes.

4.4 CHAPTER SUMMARY

In this chapter we have successfully introduced a new BbDS scanning method of examining material state change within a composite. This method is ideal for predicting the location of damage within a composite structure and determining if damage interaction has occurred between two or more damaged areas. Using a roller electrode and base electrode is a promising setup for damage distribution in industrial applications. We have also seen that the permittivity response of a composite material will vary at

different locations of a composite specimen. This information can be further examined to determine the damage induced local property variation within a composite structure.

Finally, we have demonstrated that dielectric response varies with the change in damage mode. In this chapter we have shown that this can be proven by taking ex-situ BbDS measurements of our specimens while loading and unloading the specimen with a tensile force. In chapter 5, we will briefly explain our future plans to show these variations by taking in-situ measurements as well.

CHAPTER 5

CONCLUSIONS AND FUTURE INNOVATIONS

Engineered materials are evolving into more complex formulations and are being used in a wide variety of applications. In this work we have shown that we can characterize the changes in heterogeneous material microstructure by their dielectric variables. Broadband dielectric spectroscopy (BbDS) is proven to be a valuable method in capturing dielectric property changes in composite materials. This technique can be used on a wide variety of materials; dielectric properties of SOFC ceramic materials, glass fiber reinforced composite materials, and carbon fiber reinforced composite materials have all been effectively quantified using broadband dielectric spectroscopy. The sensitivity of the dielectric response seen at low frequency regions (0.1Hz) is very high. We are able to capture very small change in the microstructure of our materials. We have proven that we are able to capture matrix damage, fiber breaks and delamination in composite materials and we are able to capture changes in porous microstructure of ceramic materials.

Ceramic materials for solid oxide fuel cells (SOFC) can be characterized by their dielectric properties and by using a 3-D X-ray microscope and image processing techniques. The porous structure of the ceramic material can then be segmented and quantified. The microstructure geometry can then be linked to the dielectric variables for that structure. This means of characterization will not only focus on porosity but also

determine how factors such as pore size and shape affect the dielectric variables of solid oxide fuel cell materials. In future work we would like to model how these changes in microstructure effect dielectric variables by inserting segmented images into a finite element modeling and simulation software.

We have shown that the change in microstructure of two different composite materials can be effectively captured using broadband dielectric spectroscopy. The two different materials clearly demonstrate that these methods can be used on both insulating composite material (glass-fiber/epoxy composites) and predominantly dielectric composite materials (carbon-fiber polymer matrix composites). For both of these materials we were able to detect the changes in microstructure due to low velocity impact. These changes include matrix damage and clear fracture path formation throughout the structure. We were successfully able to relate the changes in dielectric variables to the changes in mechanical properties, which was demonstrated to be a very useful tool for modeling and prediction of stiffness and strength degradation due to impact. This damage can then be visualized through the use of a 3D X-ray microscope. In future work, we would like to develop a consistent method of segmenting the damage seen in the 3D X-ray image. We would like to use image segmentation techniques to better visualized all damage modes and quantify the damage seen in the carbon fiber composite structures due to impact with a numerical value, such as delamination volume. In the future we would like to relate delamination volume due to impact to dielectric properties as well.

In this work we have demonstrated a new technique of taking dielectric measurements. In the past, bulk measurement proven to be a useful technique of

capturing microstructural changes in heterogeneous materials. However, the bulk measurements do not specify exact damage location and are less likely to precisely capture the interaction of damaged locations inside the material. The new line scanning BbDS method allows for visual representation of where damage is present inside the structure. The variation in BbDS response indicates damage area within the specimen and interaction between impacted locations. In the future we would like to further develop this technique so it can be practically used in manufacturing and other applications. To do so we will refine the scanning system so that the line scanner is automated and can continuously scan a large composite structure.

The static tensile tests done on two different carbon fiber composite layups indicate that sensitivity of BbDS measurements has the ability to differentiate between different damage modes. The measurements for these tests have been done ex-situ, but in-situ measurements can also be done as demonstrated by Raihan et al [7]. This is done by taking BbDS measurements while simultaneously applying a load on the specimen using the MTS machine. We would like to continue to examine the behavior of dielectric properties as the microstructure of composite materials change from a number of different loading conditions. Using this method we would also like to examine the change in dielectric properties over a long period of time. This can be done by performing tensile fatigue tests on the specimens while the BbDS response is being recorded.

Finally, in this work we have successfully demonstrated that the dielectric response is dependent upon the position of delamination throughout the plies of a specimen. This was done using specimens with controlled delamination location and a specific layup. Future work will not only consist of proving this theory for different fiber

layups, but will also consist of moving on to predicting delamination location in specimens that have been subject to loading. Microstructure analysis through 3D X-ray microscopy will then validate these predictions.

The work in this thesis is part of very broad ongoing work in the group, and we intend to continue to explore new avenues and techniques for using BbDS to capture the change in microstructure within engineered materials. These techniques are precise, non-destructive and cost effective. We can ultimately determine that dielectric variables can effectively be used in various types of materials to predict damage area and damage modes and/or effectively relate then to mechanical property degradation. These models and techniques are a promising solution for problems related to composite behavior prediction in the aerospace industry.

REFERENCES

[1] R. Raihan, Q. Lui, K. Reifsnider, F. Rabbi, Nano-Mechanical Foundations and Experimental Methodologies for Multiphysics Prognosis of Functional Behaviour in Heterogeneous Functional Materials, 23rd international congress of theoretical and applied mahcanics, 2014, 285-293

[2] W. Chiu, A. Virkar, F. Zhao, K. Reifsnider, G. Nelson, F. Rabbi, Q. Lui, HeteroFoaMs: Electrode Modeling In NanoStructured Heterogeneous Materials for Energy Systems, Journal of Fuel Cell Science and Technology, 9 (2012)

[3] R. O'Hayre, S. Cha, W. Colella, F. B. Prinz, Fuel Cell Fundamentals, John Wiley and Sons, copyright 2009

[4] F. Campbell, Structural Composite Materials, Copyright 2010, ASM International

[5] K. Reifsnider, S. Case, and J. Duthoit, The mechanics of composite strength evolution. Composites Science and Technology, 2000. 60(12-13): p. 2539-2546.

[6] U. Polomeno, M. Meo, Detecting berely visible impact damage detection on aircraft structures.

[7] R. Raihan, K. Reifsnider, D. Cacuci, Q. Liu, Dielectric signatures and Interpretive Analysis for Changes of State in Composite Materials, Wiley Online Library, March 2015

[8] J. Baker, J.M. Adkins, F. Rabbi, Q. Liu, K. Reifsnider, R. Raihan, Meso-design of Heterogeneously Dielectric Material Systems: Structure property relationships, Journal of Advanced Dielectrics, Vol.4, No. 2, 2014, 1450008.1 – 1450008.9

[9] A. Volkov, A. Prokhorov, Broadband Dielectric Spectroscopy of Solids, Radiophysics and Quantum Electronics, Vol. 46, Nos. 8-9, 2003

[10] Y. Chen, Fabrication and Characterization of Novel Electrodes for Solid Oxide Fuel Cell for Efficient Conversion, University of South Carolina, 2014

[11] P. Majumdar, M. Raihan, K. Reifsnider, F. Rabbi, Effect of Porous Electrode Morphology on Broadband Dielectric Characteristics of SOFC and Methodologies for Analytical Predictions, ASME 2011

[12] A. Lanzini', P. Leone, P. Asinari, Microstructural Characterization of Solid Oxide Fuel Cell Electrodes by Image Analysis Technique, Journal of Power Sources, 2008, 194(1): p.408-422

[13] E. Tuncer, S. Gubanski, Dielectric Mixtures: Electrical Properties and Modeling IEEE, Transactions on Dilectric and Electrical Insulation, 2002, 9(5): p.809-828

[14] Z. Hashian, Analysis of Stiffness Reduction of Cracked Cross-ply Laminates, Eng Fract Mech 1986; 25(5-6):771

[15] J. Koo, J Choi, C. Soak, Prediction of Post-Impact Residual Strength and Fatigue Characteristics after Impact of CFRP Composite Structures, Composites: Part B, 2014; 60(B) 300-306

[16] G. Capirno, Residual Strength Prediction of impacted CFRP laminates, J Compos Mater 1984; 18:2269

[17] G. Davies, D. Hitchings, G. Zhou, Impact Damage and Residual Strengths of Woven Fabric Glass/Polyester Laminates, Composites: Part A, 1996; 27 (A):1147

[18] J. Koo, J. Choi, C. Seok, Evaluation for Residual Strength and Fatigue Characteristics after Impact in CFRP composites, Compos Struct, 2013;105:53

[19] F. Kremer, A. Schonhals, Broadband Dielectric Spectroscopy, Sringer-Verlag Berlin Heidelberg, Copyright 2003

[20] S. Kessler, S. Spearing, M Atalla, C. Cesnik, C. Soutis, Damage Detection in Composite Materials using Frequency Response Methods, Composites Part B Engineering, 2002

[21] Y. Zou, L. Tong, P. Steven, Vibration-Based Model-Dependent Damage Identification and Health Monitoring for Composite Structures, Journal of Sound and Vibration, 2000; 2(230) p357-378

[22] S. Valzed, C. Soutis, Delamination Detection in Composite Laminates from Variations of Their Modal Characteristics, Journal of Sound and Vibration, 1999; 1(228), p1-9

[23] R. Raihan, J.M. Adkins, J. Baker, F. Rabbi, K Reifsnider, Relationship of Dielectric Property Change to Composite Material State Degradation, Composite Science and Technology 105, 2014

[24] S. Ogihara, K. Reifsnider, Characterization of Nonlinear Behavior in Woven Composite Laminates. Applied Composite Materials, 2002. 9(4): p. 249-63.

[25] K. Reifsnider, and S.W. Case, Damage Tolerance and Durability of Material Systems. 2002, New Tork: John Wiley & Sons, Inc.

[26] K. Reifsnider, The critical element model: A Modeling Philosophy. Engineering Fracture Mechanics, 1986. 25(5-6): p. 739-749.

[27] K. Reifsnider, Z. Gao, A Micromechanics Model for Composites Under Fatigue Loading. International Journal of Fatigue, 1991. 13(2): p. 149-156.

[28] K. Reifsnider, R. Jamison, Fracture of Fatigue-loaded Composite Laminates. International Journal of Fatigue, 1982. 4(4): p. 187-197.

[29] K. Reifsnider, A. Talug, Analysis of Fatigue Damage in Composite Laminates. International Journal of Fatigue, 1980. 2(1): p. 3-11.

[30] S. Subramanian, K. Reifsnider, W. Stinchcomb, A Cumulative Damage Model to Predict the Fatigue Life of Composite Laminates Including the Effect of a Fibre-Matrix Interphase. International Journal of Fatigue, 1995. 17(5): p. 343-351.

[31] V. Tamuzs, K. Dzelzitis, K. Reifsnider, Prediction of the Cyclic Durability of Woven Composite Laminates. Composites Science and Technology, 2008. 68(13): p. 2717-21.

[32] P. Gokulanandam, Homogenization based Continuum Damage Models for Composites under Monotonic and Cyclic Loading, in Mechanical Engineering. MS Thesis (2011), Ohio State University: Columbus, OH.

[33] Y. Lin, S. Zhongqing, L. Ye, Guided Lamb Waves for Identification of Damage in Composite Structures: A Review. Journal of Sound and Vibration, 2006. 295(3-5): p. 753-80.

[34] R. Talreja, Damage and Fatigue in Composites - A Personal Account. Composites Science and Technology, 2008. 68(13): p. 2585-2591.

[35] P. Fazzino, K. Reifsnider, P. Majumdar, Impedance Spectroscopy for Progressive Damage Analysis in Woven Composites. Composites Science and Technology, 2009. 69(11-12): p. 2008-14.

[36] K. Reifsnider, Material State Changes as a Basis for Prognosis in Aeronautical Structures. Aeronautical Journal, 2009. 113(1150): p. 789-798.

[37] P. Fazzino, K. Reifsnider, Electrochemical Impedance Spectroscopy Detection of Damage in Out of Plane Fatigued Fiber Reinforced Composite materials. Applied Composite Materials, 2008. 15(3): p. 127-138.

[38] K. Reifsnider, P. Majumdar, Material State Change Relationships to Fracture Path Development for Large-Strain Fatigue of Composite Materials. Mechanics of Composite Materials, 2011. 47(1): p. 1-10.

[39] E. Bogatin, D. DeGroot, S. Gupta, Frequency Dependent Material Properties, in DesignCon 2010. 2010: Santa Clara, CA

[40] P. Huray, The Foundations of Signal Integrity. November 2009: Wiley-IEEE Press.

[41] M. Ozcan, Characterization of Frequency-Dependent Material Properties of Human Liver and its Pathologies using an Impact Hammer. Medical Image Analysis, 2011. 15(1): p. 45-52.

[42] P. Fazzino, K. Reifsnider, Electrochemical Impedance Spectroscopy Detection of Damage in Out of Plane Fatigued Fiber Reinforced Composite Materials. Applied Composite Materials, 2008.